Bachelor Thesis
Time-Resolved Phase-Sensitive Detections for Quantum Fluids of Light

Submitted by

Marc YOUNES
Bachelor of Science
Ecole Polytechnique

Under the guidance of

Quentin GLORIEUX
Associate Professor
Laboratoire Kastler Brossel, Sorbonne Université

Acknowledgements

This thesis would not have been possible without the support of many individuals.

I would like to express my sincere gratitude to my supervisor, Professor *Quentin Glorieux* for first and foremost his trust and support without which the project would have not been set. His guidance, advice and help during the project were essential.

I am also particularly grateful to have had the chance to work closely with Doctoral Student *Myrann Baker Rasooli* with whom I had very insightful conversations from physics to daily life on a day-today basis.

I cannot forget to thank the rest of the Rubidium team, Postdoctoral Researcher *Devang Naik*, as well as Doctoral Students *Clara Piekarski*, *Quentin Schibler*, *Simon Lepleux*, *Alix Merolle* and *Sukhman Singh* which were always present for giving new insights and ideas. I also extend gratitude to Doctoral Student *Killian Guerrero*, and the rest of the Polaritons and Nano teams for their close help. Thank you for the amazing time. I hope your blood sugar levels are not very high after the Lebanese sweets.

I thank ex-PhD student Tangui Aladjidi for his contributions to the NLSE Package without which the numerical parts of this project would have not happened. His thesis also served as a great pedagogical material to get used to the concepts before embarking in this project.

I can confidently say that this thesis allowed me to learn a lot academically, but most importantly the approach of Professor *Quentin Glorieux* as well as the spirit of the group taught me values that I will always hold in my scientific journey, from laboratory ethics to communication.

I would also like to thank Pr. Iacopo Carusotto for an interesting theoretical discussion.

Additionally, I extend my gratitude to everyone involved in the Bachelor of Science Program, notably the people who provided the foundations for such an opportunity:
Dean *Christophe Josserand*, referent instructor *Jean-Eric Wegrowe* and third year officer *Lorraine Wowo*.

I am also indebted to my family, as well as every teacher, professor and lecturer that shared with me part of their understanding of this world. Without their guidance, the curiosity driving me to follow this path wouldn't have been fostered.

Abstract

Quantum fluids of light emerged recently as a way to study quantum many-body phenomena. Through a mapping between the equations governing 2D quantum fluids, notably the Gross-Pitaevskii Equation, and the Non-Linear Schrödinger Equation governing the propagation of light in Kerr media, we can draw parallels between the two systems. In our case, we specifically study the propagation of light through a hot rubidium vapor cell. In such a paraxial fluid of light, the propagation direction plays the role of an effective time. In this thesis, after exploring this mapping, we study the dynamics of vortices which are common to both systems. Such dynamics include splitting, spontaneous and stimulated emission of waves. Going from a linear medium (air) to a non-linear medium (hot atomic vapor) through the cell interface suddenly increases interactions, thus driving the system out of equilibrium. This creates perturbations that we can observe in the fluid, known as quenches. As we would be interested to study vortex dynamics in the equilibrium case, and since we believe quenches might affect vortex dynamics, we explore two possible ideas to eliminate these perturbations: ramping interactions adiabatically or injecting "antiquenches". We also test some of the numerical tools developed by a study of superradiance.

Contents

1   Introduction

With the emergence of the field of many body quantum physics, a lot of effort has been put to study collections of quantum particles over the past decades. One of the most fundamental predictions was that bosonic particles would condense if they were cooled below a critical temperature. Cooling techniques, developed by Claude Cohen-Tannoudji, Steven Chu and William D. Phillips paved the way for experiments in this field and granted them the Nobel prize in 1997 [1, 2, 3]. These discoveries allowed the observation of the theorized Bose-Einstein condensates (BEC) in 1995 by the NIST-JILA lab [4, 5]. This phenomenon has also been tightly associated with superfluidity. As the atoms condense, they behave collectively. They are thus governed by the evolution of one wavefunction, described by the **Gross-Pitaevskii Equation** (GPE) [6, 7].

The GPE is an instance of the **Non-Linear Schrödinger Equation** (NLSE), which is a non-linear differential equation relevant to multiple fields of physics. In the context of non-linear optics, the NLSE describes the evolution of electric field envelopes in a medium with $\chi^{(3)}$ non-linearity. Thus, from a mathematical perspective, the NLSE and the GPE are basically the same. This leads to the field of **Quantum Fluids of Light**. A lot of analogies can be drawn between BEC physics and non-linear optics. Because this correspondence, one can be used to study the other. In practice, it becomes a question of which system is easier to study. The advantage of Quantum fluids of light is that optics, being an older, well-studied field, offers a wide platform for ideas to test. Quantum fluids of light can be studied in different systems, such as in confined geometries for example. However, in this thesis, we work with simpler cavityless paraxial systems using hot atomic vapor cells (specifically, Rubidium vapors).

The work in this thesis is mainly focused on studying numerically vortex dynamics and quenches in these systems.
In **Section 2**, the theoretical foundations necessary to understand the analogy between the GPE and the NLSE is provided. Bogoliubov theory is introduced. The numerical framework for the NLSE solver is also described.
In **Section 3**, the concept of vortices is explained. Some of their dynamics such as splitting are also explored.
In **Section 4**, interaction quenches are described. To study vortex dynamics rigorously, eliminating quenches is interesting. Possible methods to achieve this are hence introduced.
In **Appendix A**, superradiance, whose outcomes are known, is also used as a means to test the developed numerical tools.

A lot of numerical tools have been developed during this thesis. These can be found on:
`https:\` to add when github is cleaned

2 Quantum Fluids of Light

In this Section, we will focus on describing the theoretical background needed to understand the mapping between the GPE and the NLSE. The numerical method used to solve the latter will be described. Bogoliubov theory will also be briefly introduced. We will follow similar derivation steps as Tangui Aladjidi's PhD Thesis and its references [8] as well as the review in Ref.[9].

2.1 Light Propagation in a Non-linear Medium

For our purposes, to describe the evolution of the electric field envelope in a Kerr medium, it is enough to start using a classical approach. Using Maxwell's equations, it can be shown that the propagation of an electric field $\mathbf{E}$ in a medium with electronic polarization $\mathbf{P}$ follows Helmholtz's equation [10]:

$$\nabla^2 \mathbf{E} - \frac{1}{c^2}\frac{\partial^2 \mathbf{E}}{\partial t^2} = \frac{1}{\epsilon_0 c^2}\frac{\partial^2 \mathbf{P}}{\partial t^2}, \tag{1}$$

where c is the speed of light in vacuum and ϵ_0 is the electric permittivity of vacuum.

In linear optics, it is enough to write $\mathbf{P} = \epsilon_0 \chi \mathbf{E}$. However, if we assume a *nonlinear, isotropic, centrosymmetric,* and *local* medium, we can expand the polarization $\mathbf{P}$ into higher-order terms of the electric field $\mathbf{E}$, neglect all even-order terms, assume that $\mathbf{P}$ is aligned along the direction of $\mathbf{E}$, and consider that the polarization at any given position depends only on the electric field at that same position. It is important to note that the hot atomic vapors used in our case satisfy all these assumptions except *locality*, which we introduce initially for simplicity. The polarization $\mathbf{P}$, which can now be described solely by its amplitude since it is aligned with $\mathbf{E}$, can therefore be expressed in the frequency domain. In the *frequency degenerate* case (where only one frequency is involved) we have:

$$P(\mathbf{r}, \omega) = \epsilon_0 \left(\chi^{(1)}(\mathbf{r}, \omega)E(\mathbf{r}, \omega) + 3\chi^{(3)}(\mathbf{r}, \omega)|E(\mathbf{r}, \omega)|^2 E(\mathbf{r}, \omega) \right). \tag{2}$$

Now, we assume that we have a *monochromatic field*, that we can achieve for example by using a continuous wave (CW) laser (we will see shortly the implications of this assumption for the geometry of the system):

$$E(r, t) = \frac{1}{2}\left(\mathcal{E}'(r, \omega)e^{i\omega t} + \mathcal{E}'^*(r, \omega)e^{-i\omega t} \right), \tag{3}$$

Injecting Eq. 2 and Eq. 3 in Eq. 1, expanding, and ignoring terms oscillating at high frequencies (3ω) that average out over the time scales of interest, we get:

$$\nabla^2 \mathcal{E}'(\mathrm{r}, \omega) + \frac{\omega^2}{c^2}[1 + \chi^{(1)}(\omega)]\mathcal{E}'(\mathrm{r}, \omega) = -\frac{3}{4}\frac{\omega^2}{c^2}\chi^{(3)}(\omega)|\mathcal{E}'(\mathrm{r}, \omega)|^2\mathcal{E}'(\mathrm{r}, \omega). \tag{4}$$

If we decompose the refractive index in a linear part n and a non-linear part $\Delta n = 2\bar{n}_2|E|^2$, we can write

$$(n + \Delta n)^2 = 1 + \chi^{(1)} + 3\chi^{(3)}(\omega)|E|^2, \tag{5}$$

we get by expanding, comparing the coefficients in $|E|^2$, and ignoring terms higher than first order

$$n = \sqrt{1 + \chi^{(1)}} := n_0, \quad \bar{n}_2 = \frac{3\chi^{(3)}}{4n_0}. \tag{6}$$

We can also include a small local variation $\delta n(r)$ of the index of refraction so it becomes

$$n = \sqrt{1 + \chi^{(1)}} = n_0 + \delta n(r). \tag{7}$$

For experimental purposes and since it is easier to measure intensities $I = \frac{1}{2}\varepsilon_0 n_0 c |E|^2$ instead of $|E|^2$, it is convenient to redefine $\Delta n = n_2 I$, for $n_2 = \frac{2}{\varepsilon_0 c}\bar{n}_2$. We note that in our system, we will only work with n_2 negative, known as the self defocusing case. More explicitly, suppose we are working with a Gaussian beam. The intensity of such a beam is higher at its center than at the edges, hence, it will experience lower refractive index at its edges, and it will self defocus.

Now, if we define the medium wavenumber as $k := \frac{\omega}{c}\text{Re}(\sqrt{1 + \chi^{(1)}})$ and the absorption coefficient $\alpha := 2k\frac{\omega}{c}\text{Im}(\sqrt{1 + \chi^{(1)}})$, Eq. 4 becomes, assuming small losses (so we can ignore the α^2 term):

$$\nabla^2 \mathcal{E}' + k^2 \mathcal{E}' + i\alpha \mathcal{E}' = -\frac{3}{4}\frac{\omega^2}{c^2}\chi^{(3)}|\mathcal{E}'|^2 \mathcal{E}'. \tag{8}$$

Up to this point, the propagation equation (Eq. 8) still involves, through the Laplacian operator, 3 dimensions of space. This is where the *slowly-varying envelope approximation* and *paraxial approximation* play a big role in paraxial fluids of light. We will see how these approximations will reduce the system into a 2D+1 geometry, with the propagation direction acting as an effective time.

For this thesis, we will pick the z direction as the propagation direction. We will also use the symbol $\perp$ for the transverse (x, y) plane. The approximations stated above write as:

- *slowly-varying envelope approximation:* $\mathcal{E}'(\mathbf{r}) = \mathcal{E}(\mathbf{r}_\perp, z)e^{ik_0 z}$, for $k_0 = n_0\omega/c$, the envelope varies slowly along z compared to $\lambda = 2\pi/k_0$ hence decoupling tranverse from longitudinal dynamics;

- *paraxial approximation:* $\frac{\nabla_\perp^2 \mathcal{E}}{k_0^2} \sim \frac{\partial_z \mathcal{E}}{k_0} \ll 1$, the beam deviates barely from the optical axis.

With these approximations, it is straightfoward to see that the Laplacian term becomes

$$\nabla^2 \mathcal{E}' = \left(\nabla_\perp^2 \mathcal{E} - k_0^2 \mathcal{E} + 2ik_0\frac{\partial \mathcal{E}}{\partial z}\right)e^{ik_0 z}. \tag{9}$$

Injecting Eq. 9 in 8 and using all the definition above, we can get the final NLSE. Noticing that $k = k_0 + \delta k(r)$, we get the following equation describing the evolution in z, using a reduced 2D Laplacian:

Non-Linear Schrödinger Equation (NLSE)

$$i\frac{\partial \mathcal{E}}{\partial z} = \left(-\frac{1}{2k_0}\nabla_\perp^2 - i\frac{\alpha}{2} - k_0\frac{\delta n(\mathbf{r})}{n_0} - k_0\bar{n}_2|\mathcal{E}|^2\right)\mathcal{E}. \tag{10}$$

At some point in the derivation, we assumed that we work with a CW laser with a negligible spectral extent. The electric field would thus basically be a plane wave in the z direction. We therefore get translational invariance reducing the system to a 2D+1 geometry. On the other hand, to get a 2D+1 quantum fluid, we only need physical confinement along the z direction and real-time would still act as the effective time. We note that if we chose to work with pulsed/non-monochromatic light, dispersion would have modified the 2D+1 geometry as we would need to introduce extra terms, involving real-time derivatives, to take it into account (see Chap. 1 of Ref. [8] for more details).

As mentioned earlier, the NLSE governing our optical system is very similar to the GPE governing weakly interacting Bose gases, defined as follows:

Gross-Pitaevskii Equation (GPE) in 2D

$$i\hbar\frac{\partial \psi}{\partial t} = \left(\frac{-\hbar^2}{2m}\nabla_\perp^2 + i\gamma + V(\mathbf{r}) + g|\psi|^2\right)\psi, \tag{11}$$

---

where $g = \frac{4\pi\hbar^2 a_s}{m}$, with a_s the s-wave scattering length, $V(\mathbf{r})$ a potential energy term (e.g. trapping potential), and γ is a loss term. Our goal is to now draw the parallelisms between the two equations. Identifying term by term, we get the following correspondences.

- **Diffraction** $-\frac{1}{2k_0}\nabla_\perp^2 \leftrightarrow -\frac{\hbar^2}{2m}\nabla_\perp^2$ **Kinetic Energy**.
  The photons acquire an an effective mass $\bar{m} = \frac{\hbar k_0}{c}$.

- **Absorption** $-i\frac{\alpha}{2} \leftrightarrow i\gamma$ **Losses**.

- **Refractive Index Spatial Modulation** $k_0\frac{\delta n(\mathbf{r})}{n_0} \leftrightarrow V(\mathbf{r})$ **Potential Energy**.
  An effective potential is defined as $\bar{V} = \frac{-\hbar c k_0 \delta n(\mathbf{r})}{n_0}$.

- **Non-Linear Refractive Index** $k_0\bar{n}_2|\mathcal{E}|^2 \leftrightarrow g|\psi|^2$ **Interaction Energy**.
  $\chi^{(3)}$ nonlinearity mediates an effective interaction between photons $\bar{g} = -\hbar c k_0\bar{n}_2$.

The 2D dynamics of the electric field envelope propagating along z in a Kerr medium can be comparable to those of the many-body wavefunction in real-time t. We can thus say that the propagation direction z acts as an effective time $\tau = \frac{z}{c}$. Fixing z is equivalent to fixing time.
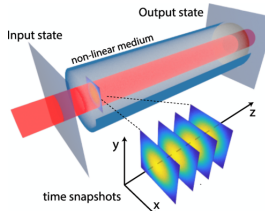
Figure 1: In a paraxial fluid of light, the electric field envelope of light traveling in a Kerr medium follows the NLSE which is analogous to the GPE, with the propagation direction z acting as an effective time $\tau = z/c$. Taking transverse snapshots at specific z and superposing them would form a video of the evolution of a quantum fluid. Image adapted from Ref. [11].

2.2 Numerical analysis using a NLSE Solver

To solve numerically the NLSE, ex-PhD student Tangui Aladjidi and PhD student Clara Piekarski developed a python package [1] detailed in Ref. [8, 12].

The package uses a split-step spectral scheme to solve NLSE efficiently. We will see that this method is matricial by essence and thus works best when working on GPU.

The first step is to, as done in most numerical partial differential equations solvers, discretize space and (effective) time. The electric field thus becomes a pixelized 2D array $E_{i,j} = E(x_i, y_j)$, where the distance between x_{i+1} and x_i, y_{i+1} and y_i is fixed by the number of pixels N and the cell window size w we choose; we get a pixel size $p = w/N$. The simulation is also done at steps δz. The simulation precision increases when the discretization is smaller, at the expense of higher simulation time. For most applications, $N = 2048$, $w = 20 \times 10^{-3}m$, $p = 9.7 \times 10^{-6}m$ and $\delta z = 10^{-4}m$ give a good compromise between accurate simulations and reasonable simulation times (of the order of a minute at maximum on the group's GPU *Hawking*). These parameters will be the default ones for this thesis except stated otherwise. Depending on the need, we will also crop or not a part of the array and keep areas of interest.

In fact, the operators involved in the NLSE 10 can be split as follows:

$$\frac{\partial \mathcal{E}}{\partial z} = \left(\underbrace{-\frac{1}{2k_0}\nabla_\perp^2}_{\mathcal{D}} \underbrace{-i\frac{\alpha}{2} + k_0\delta n + k_0\bar{n}_2|\mathcal{E}|^2}_{\mathcal{N}} \right)\mathcal{E}. \tag{12}$$

We thus define a linear $\mathcal{D}$ operator whose application is easy to solve in Fourier space (due to the Laplacian) and a non-linear $\mathcal{N}$ operator whose application is easy to solve in real space.
Effective time propagation for small steps hence gives

$$\mathcal{E}(z + \delta z) = \mathcal{E}(z)e^{i\delta z(\mathcal{D}[\mathcal{E}(z)] + \mathcal{N}[\mathcal{E}(z)])}. \tag{13}$$

Since we are dealing with operators, to exploit the usual properties of the exponential (such as decomposing a sum in the exponent into a product of exponentials), the operators should commute, which is not straightforward here. The trick is thus to use the Baker–Campbell–Hausdorff formula after noticing that we are propagating at small steps δz to get

$$\mathcal{E}(z + \delta z) \approx \mathcal{E}(z)e^{i\delta z\mathcal{D}[\mathcal{E}(z)]}e^{i\delta z\mathcal{N}[\mathcal{E}(z)]}. \tag{14}$$

Knowing this, the algorithm becomes straightforward and requires going back and forth between Fourier and real space: 1) Fourier transform, 2) apply the linear propagator operator term, 3) inverse Fourier transform, 4) apply the non-linear operator propagator term and 5) loop over.
In practice, we can for example get for any integer multiple of δz, 2D arrays of the electric field of any input that we can define analytically. Experimentally this is achieved using a Spatial Light Modulator (SLM) and a camera at the end of the cell. We can then use this to analyze intensity, phase, and any quantity related to the electric field as seen in Fig. 2. We note that for an electric field at position x_m, y_n, with phase $\phi_{m,n}$ and of the form $E_{m,n} = A_{m,n}e^{i\phi_{m,n}}$, we define for simplicity the intensity, in a.u. as $|E_{m,n}|^2$.

---

[1]The documentation can be found on `https://quantum-optics-lkb.github.io/NLSE/`

Except stated otherwise, we will show images where each pixel corresponds to a coefficient; the ticks on the axes will thus label the pixel number.
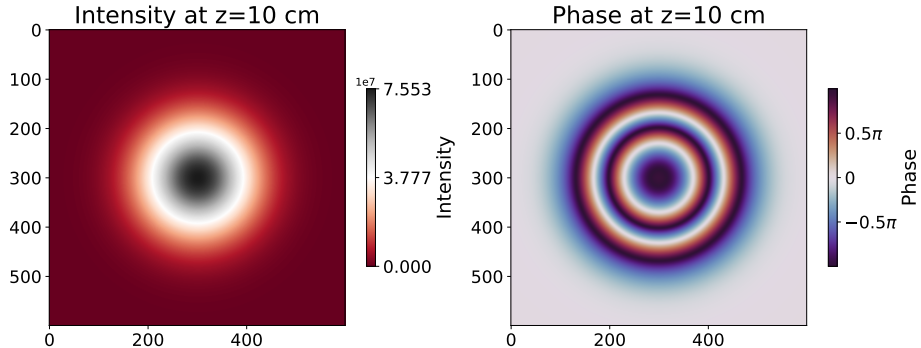
Figure 2: Intensity and Phase diagrams at $z = 10cm$ for a Gaussian input field $\psi_0 = e^{-(x^2+y^2)/w_0^2}$ with waist $w_0 = 1.7 \times 10^{-3}m$. The axes are labeled by pixel number, with pixel size $p = \frac{w}{N} = 9.7 \times 10^{-6}m$.

2.2.1 Numerical Tool: Absorbing Boundary Conditions

To efficiently Fourier transform on a classical computer, the Fast Fourier Transform (FFT) is the most known efficient algorithm. It is used in the NLSE package. However, the FFT assumes that the input is periodic over the computational domain. In our case, the physical problem does not always exhibit periodicity. Therefore, the FFT enforces an artificial periodic extension. This can lead to discontinuities at the edges of the simulation domain, where the actual field values abruptly transition from the physical domain to the artificially repeated values. Such discontinuities introduce high-frequency components when transformed into the frequency domain, which then appear as non-physical reflections in the spatial domain. Essentially, when a wave approaches a boundary under these conditions, it interacts with its mirrored counterpart due to the periodic extension, resulting in an artificial reflection that contaminates the simulation results. This effect becomes highly significant when the window size approaches the beam waist size as can be seen in Fig. 3.

6

(a)

Intensity at z=10 cm   Phase at z=10 cm

(b)

Intensity at z=10 cm   Phase at z=10 cm
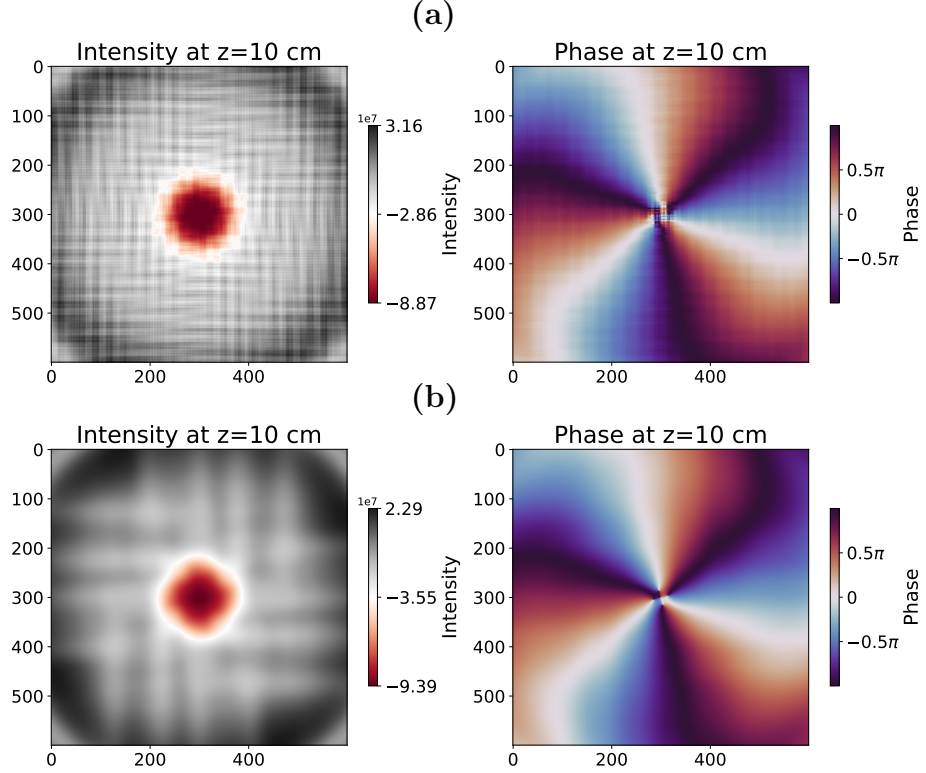
Figure 3: Intensity and phase diagrams at $z = 10cm$ for a gaussian background ψ_0 multiplied by an input vortex field $\psi_v(r,\theta) = \frac{r}{\sqrt{r^2+(\frac{\xi}{0.83})^2}}e^{i\ell\theta}$ of charge $l = 3$ and healing length $\xi = 17 \times 10^{-6}m$ (see Section 3 for more details). **(a)** Simulation for the classical NLSE code with window $w = 2w_0$. **(b)** Simulation for the modified NLSE cose using the Absorbing Boundary Conditions method with an absorption width of $0.3w$. For both figures, the background intensity and phase are subtracted, hence explaining the negative intensities.

To solve this issue, two main possible solutions exist. The first and more complex one is known as the Perfectly Matched Layers (PML) method. However, the one that we use is the absorbing boundary conditions method. We implement it by first initializing all matrix coefficients to 1. Then, we define an absorption width W defined by its distance from the boundary. The pixels, from the four sides, go from 1 to 0 at the boundary following a specific parametrization (in that case we defined it for the x direction and for an absorption width W as $cos^2((x-N-W)\frac{\pi}{2W})$ It is defined similarly for y. The obtained matrix is later multiplied by the normalized electric field to define a new normalized electric field matrix decaying to 0 on the boundaries. Fig. 3 already shows improvements in terms of reflections for an extreme case of small window. Fine tuning the absorption width can yield better results.

2.3 Hydrodynamic Formulation

Since many of the dynamics we study in a quantum fluids of light system are common to fluid mechanics, it is useful to adopt a hydrodynamic formulation. Using the Madelung transform [13], we redefine the electric field envelope as

$$\mathcal{E}(\mathbf{r}_\perp, z) = \sqrt{\rho(\mathbf{r}_\perp, z)}e^{i\Phi(\mathbf{r}_\perp, z)}. \tag{15}$$

The velocity of the fluid would thus be defined as

$$\mathbf{v} = \frac{c}{k_0}\nabla\phi = \frac{\hbar}{\bar{m}}\nabla\phi. \tag{16}$$

Plugging Eq. 15 in Eq. 10, we get a quantum version of Euler equations:

$$\frac{\partial\rho}{\partial z} + \frac{1}{c}\nabla_\perp.(\rho\mathbf{v}) = -\alpha\rho$$
$$\frac{\partial\mathbf{v}}{\partial z} + \frac{1}{2c}\nabla_\perp\mathbf{v}^2 + \frac{c}{k_0}\nabla_\perp\left(\bar{g}\rho + \bar{V} - \frac{1}{2k_0}\frac{\nabla^2\sqrt{\rho}}{\sqrt{\rho}}\right) = 0. \tag{17}$$

The last term is known as the quantum pressure term and is not present in the classical formulation of Euler equations.

2.4 Bogoliubov Theory

In Subsection 2.2, we already explored a way to solve the NLSE numerically. The NLSE (or equivalently GPE) can however not be solved trivially without approximations and initial guesses. This is where Bogoliubov theory comes into play. Without detailing all the calculations, we will show the steps to retrieve the **Bogoliubov dispersion relation**. We will now switch to a quantum treatment. In fact, it can rigorously be shown (consult Ref. [14, 15]) that the quantum formulation of NLSE yields the same equation, but now with field operators.

$$i\frac{\partial\hat{\mathcal{E}}}{\partial z} = -\frac{1}{2k_0}\nabla_\perp^2\hat{\mathcal{E}} - i\frac{\alpha}{2}\hat{\mathcal{E}} + \bar{V}(\mathrm{r}, z)\hat{\mathcal{E}} + \bar{g}(\mathrm{r}, z)\hat{\mathcal{E}}^\dagger\hat{\mathcal{E}}\hat{\mathcal{E}}. \tag{18}$$

The first step is to consider a perturbative approach where we consider small quantum fluctuations $\delta\hat{\mathcal{E}}$ on top of a classical mean field $\mathcal{E}_0$ as:

$$\hat{\mathcal{E}} = \mathcal{E}_0 + \delta\hat{\mathcal{E}}. \tag{19}$$

Injecting Eq. 19 in Eq. 18, then ignoring high order terms in the perturbation, we get:

$$i\frac{\partial\delta\hat{\mathcal{E}}}{\partial z} = -\frac{1}{2k_0}\nabla_\perp^2\delta\hat{\mathcal{E}} + \bar{g}(\mathbf{r}, z)\left[2|\mathcal{E}_0|^2\delta\hat{\mathcal{E}} + \mathcal{E}_0^2\delta\hat{\mathcal{E}}^\dagger\right] - i\alpha\delta\hat{\mathcal{E}}. \tag{20}$$

Noticing that the fluctuation operators can be expressed as

$$\delta\hat{\mathcal{E}}(\mathbf{r}_\perp, z) = \int d\mathbf{k}_\perp \hat{a}_{\mathbf{k}_\perp}(z)e^{i\mathbf{k}_\perp \cdot \mathbf{r}_\perp}$$
$$\delta\hat{\mathcal{E}}^\dagger(\mathbf{r}_\perp, z) = \int d\mathbf{k}_\perp \hat{a}_{-\mathbf{k}_\perp}^\dagger(z)e^{i\mathbf{k}_\perp \cdot \mathbf{r}_\perp} \tag{21}$$

we get the following system

$$i\partial_z \begin{pmatrix} \hat{a}_{\mathbf{k}_\perp} \\ \hat{a}^\dagger_{-\mathbf{k}_\perp} \end{pmatrix} = \begin{pmatrix} -\frac{\mathbf{k}_\perp^2}{2k_0} + 2\bar{g}|\mathcal{E}_0|^2 - i\frac{\alpha}{2} & \bar{g}\mathcal{E}_0^2 \\ \bar{g}\mathcal{E}_0^{*2} & -\frac{\mathbf{k}_\perp^2}{2k_0} + 2\bar{g}|\mathcal{E}_0|^2 - i\frac{\alpha}{2} \end{pmatrix} \begin{pmatrix} \hat{a}_{\mathbf{k}_\perp} \\ \hat{a}^\dagger_{-\mathbf{k}_\perp} \end{pmatrix}. \tag{22}$$

We rewrite these coupled equations

$$i\partial_z \begin{pmatrix} \hat{a}_{\mathbf{k}_\perp} \\ \hat{a}^\dagger_{-\mathbf{k}_\perp} \end{pmatrix} = \begin{pmatrix} A - i\frac{\alpha}{2} & B \\ B^* & A - i\frac{\alpha}{2} \end{pmatrix} \begin{pmatrix} \hat{a}_{\mathbf{k}_\perp} \\ \hat{a}^\dagger_{-\mathbf{k}_\perp} \end{pmatrix}, \tag{23}$$

with

$$A := -\frac{\mathbf{k}_\perp^2}{2k_0} + 2\bar{g}|\mathcal{E}_0|^2, B := \bar{g}\mathcal{E}_0^2. \tag{24}$$

We introduce new operators defined, for a normalization that we choose to satisfy $u_{\mathbf{k}_\perp}^2 - v_{\mathbf{k}_\perp}^2 = 1$, by the system

$$\begin{aligned} \begin{pmatrix} \hat{a}_{\mathbf{k}_\perp}(z) \\ \hat{a}^\dagger_{-\mathbf{k}_\perp}(z) \end{pmatrix} &= \begin{pmatrix} u_{\mathbf{k}_\perp}(z) & v_{\mathbf{k}_\perp}(z) \\ v_{\mathbf{k}_\perp}(z) & u_{\mathbf{k}_\perp}(z) \end{pmatrix} \begin{pmatrix} \hat{b}_{\mathbf{k}_\perp}(z) \\ \hat{b}^\dagger_{-\mathbf{k}_\perp}(z) \end{pmatrix} \\ \begin{pmatrix} \hat{b}_{\mathbf{k}_\perp}(z) \\ \hat{b}^\dagger_{-\mathbf{k}_\perp}(z) \end{pmatrix} &= \begin{pmatrix} u_{\mathbf{k}_\perp}(z) & v_{\mathbf{k}_\perp}(z) \\ v_{\mathbf{k}_\perp}(z) & u_{\mathbf{k}_\perp}(z) \end{pmatrix}^{-1} \begin{pmatrix} \hat{a}_{\mathbf{k}_\perp}(z) \\ \hat{a}^\dagger_{-\mathbf{k}_\perp}(z) \end{pmatrix} \end{aligned} \tag{25}$$

designed to evolve following the equations below (we want to find new operators that are eigenmodes of the evolution):

$$\begin{aligned} \frac{\partial \hat{b}_{\mathbf{k}_\perp}}{\partial z} &= i\Omega_B(\mathbf{k}_\perp, z)\hat{b}_{\mathbf{k}_\perp} \\ \frac{\partial \hat{b}^\dagger_{-\mathbf{k}_\perp}}{\partial z} &= -i\Omega_B^*(\mathbf{k}_\perp, z)\hat{b}^\dagger_{-\mathbf{k}_\perp} \end{aligned} \tag{26}$$

(where Ω_B is a constant) called the Bogoliubov frequency. From the original system, we have

$$\begin{aligned} i\partial_z \hat{a}_{\mathbf{k}_\perp} &= \left(A - i\frac{\alpha}{2}\right)\hat{a}_{\mathbf{k}_\perp} + B\hat{a}^\dagger_{-\mathbf{k}_\perp}, \\ i\partial_z \hat{a}^\dagger_{-\mathbf{k}_\perp} &= B^*\hat{a}_{\mathbf{k}_\perp} + \left(A - i\frac{\alpha}{2}\right)\hat{a}^\dagger_{-\mathbf{k}_\perp}. \end{aligned} \tag{27}$$

Taking the z-derivative of $\hat{b}_{\mathbf{k}_\perp}$ and using the above equations yields:

$$\begin{aligned} i\partial_z \hat{b}_{\mathbf{k}_\perp} &= i\partial_z \left(u_{\mathbf{k}_\perp}\hat{a}_{\mathbf{k}_\perp} - v_{\mathbf{k}_\perp}\hat{a}^\dagger_{-\mathbf{k}_\perp}\right) \\ &= u_{\mathbf{k}_\perp}\left[\left(A - i\frac{\alpha}{2}\right)\hat{a}_{\mathbf{k}_\perp} + B\hat{a}^\dagger_{-\mathbf{k}_\perp}\right] - v_{\mathbf{k}_\perp}\left[B^*\hat{a}_{\mathbf{k}_\perp} + \left(A - i\frac{\alpha}{2}\right)\hat{a}^\dagger_{-\mathbf{k}_\perp}\right] \\ &= \left[u_{\mathbf{k}_\perp}\left(A - i\frac{\alpha}{2}\right) - v_{\mathbf{k}_\perp}B^*\right]\hat{a}_{\mathbf{k}_\perp} + \left[u_{\mathbf{k}_\perp}B - v_{\mathbf{k}_\perp}\left(A - i\frac{\alpha}{2}\right)\right]\hat{a}^\dagger_{-\mathbf{k}_\perp}. \end{aligned} \tag{28}$$

We require this to be equal to $\Omega_B \hat{b}_{\mathbf{k}_\perp} = \Omega_B\left(u_{\mathbf{k}_\perp}\hat{a}_{\mathbf{k}_\perp} - v_{\mathbf{k}_\perp}\hat{a}^\dagger_{-\mathbf{k}_\perp}\right)$. Comparing and matching coefficients leads to the system

$$\begin{cases} \Omega_B u_{\mathbf{k}_\perp} = u_{\mathbf{k}_\perp}\left(A - i\frac{\alpha}{2}\right) - v_{\mathbf{k}_\perp}B^*, \\ \Omega_B v_{\mathbf{k}_\perp} = -u_{\mathbf{k}_\perp}B + v_{\mathbf{k}_\perp}\left(A - i\frac{\alpha}{2}\right). \end{cases} \tag{29}$$

In matrix form:

$$\begin{pmatrix} A - i\frac{\alpha}{2} - \Omega_B & -B^* \\ B & -A + i\frac{\alpha}{2} + \Omega_B \end{pmatrix} \begin{pmatrix} u_{\mathbf{k}_\perp} \\ v_{\mathbf{k}_\perp} \end{pmatrix} = \begin{pmatrix} 0 \\ 0 \end{pmatrix}. \tag{30}$$

To get consistent, non-trivial solutions for this homogeneous system, the determinant of the matrix above should vanish yielding:

$$\Omega_B(\mathbf{k}_\perp) = \pm\sqrt{\frac{\mathbf{k}_\perp^2}{2k_0}\left(\frac{\mathbf{k}_\perp^2}{2k_0} + 2\bar{g}|\mathcal{E}_0|^2\right)} - i\frac{\alpha}{2}. \tag{31}$$

This is the **Bogoliubov dispersion**. Now that we have found the eigenmodes of our evolution, we can think about the physics underlying this dispersion.

We identify two interesting regimes. Using Taylor expansions for the approximations:

- $k_\perp \ll k_0\sqrt{\Delta n}$, we get a linear dispersion $\Omega_B(k_\perp) \approx k_\perp\sqrt{\Delta n} := c_s k_\perp$. Similarly to the dispersion of sound waves, this is a sonic regime, which enables us to define a speed of sound $c_s = \sqrt{\Delta n} = \sqrt{n_2\rho}$.

- for $k_\perp \gg k_0\sqrt{\Delta n}$, we get a quadratic dispersion characteristic or particle-like systems $\Omega_B(k_\perp) \approx \frac{k_\perp^2}{2k_0}$.

As Eq. 20 is linear, the analysis above allows us to say that the perturbations can be written as a (discrete or continuous) superposition of modes of the form:

$$u_{\mathbf{k}_\perp}e^{i\mathbf{k}_\perp.\mathbf{r}_\perp}e^{-i\Omega_B(\mathbf{k}_\perp)z} - v_{\mathbf{k}_\perp}e^{-i\mathbf{k}_\perp.\mathbf{r}_\perp}e^{i\Omega_B(\mathbf{k}_\perp)z}. \tag{32}$$

For some systems, it might be interesting to work in spherical coordinates (r, ϕ, θ).
In fact, it can be shown [2] that we can expand a plane wave, for Bessel functions j_ℓ and $Y_{\ell m}$ the spherical harmonics as:

$$e^{i\mathbf{k}_\perp.\mathbf{r}_\perp} = \sum_{\ell=0}^{\infty}\sum_{m=-\ell}^{\ell} c_{\ell m}(\mathbf{k}_\perp)j_\ell(\mathbf{k}_\perp.\mathbf{r}_\perp)Y_{\ell m}(\pi/2, \theta). \tag{33}$$

Because of symmetries of some problems, such as when a vortex exists (see Section 3), it would thus be interesting to work in polar coordinates and look at modes that we label by $e^{im\theta}$ (due to the spherical harmonics). We note that we chose $\phi = \pi/2$ as we work in the transverse plane.

---

[2] As done in Lecture notes `https://scipp.ucsc.edu/~haber/ph215/PlaneWaveExpansion.pdf`. We note that in the Lecture notes, the polar coordinates are defined as (r, θ, ϕ) instead of (r, ϕ, θ) like in our case (we chose this convention for consistency with the following sections).
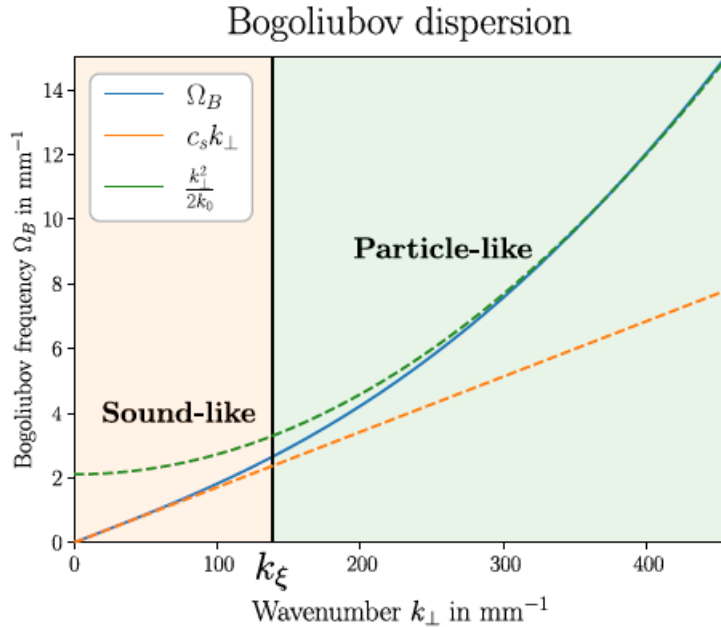
Figure 4: Theoretical Bogoliubov dispersion. When the non-linear interactions related to Δn are strong, we have a sonic regime (shaded in Orange). In the opposite case, we have particle-like dispersion (shaded in Green). Image adapted from Ref. [8].

The analysis and the Fig. 4 above also suggest that in strongly interacting regimes, perturbations should in principle propagate at the speed of sound. This will be given a particular interest in Section 4.

3   Vortices

In this Section, we will focus on the study of vortices. After defining them and exploring some of their properties, we will see how even with the simplest configurations possible (one single or multi-charged vortex), we get complex and interesting stimulated and spontaneous dynamics.

3.1   Definition and Properties

A vortex is defined as topological defect around which the fluid circulates due to a twisting in its phase. At the core of this vortex, the fluid density vanishes to account for a phase singularity. A simple classical analogy is water spiraling down a drain. However, unlike the continuous flow seen in classical fluids, quantum vortices occur in quantized steps. Vortex dynamics play a big role in multiple fields of physics from superconductor physics, topological matter, BECs, high-energy physics, etc. Many interesting phenomena can occur when considering multiple vortices at the same time, notably, they can combine with other vortices, forming for example Jones-Roberts solitons [16], rearrange themselves into a lattice [17], drive turbulent dynamics [18], etc. However, in this thesis, we will focus on the study of one single or multi-charged vortex at most.

In this Subsection, we will follow similar steps as in Chap. 9 of the 2nd edition of the book "Bose–Einstein Condensation in Dilute Gases" by C. J. Pethick and H. Smith [19]. For the sake of consistency with the book, we will use the notation of BECs using the effective quantities defined in the correspondences made in Subsection 2.1. We also choose to work in polar coordinates.

Using the hydrodynamic formulation, we can define the velocity of the fluid as:

$$\mathbf{v} = \frac{\hbar}{\bar{m}} \nabla \phi. \tag{34}$$

Unless the phase showcases a singularity (which is the case for a vortex field), the velocity is irrotational with $\nabla \times \mathbf{v} = 0$.
If we assume that we have a field with single-values, the change in its phase would be an integer multiple of 2π around a closed contour:

$$\Delta\phi = \oint \nabla\phi \cdot d\mathbf{l} = 2\pi\ell, \text{where } \ell \in \mathbb{Z}. \tag{35}$$

This condition also means that the electric field should vary as $e^{i\ell\theta}$. This gives us a circulation quantized in units of $\frac{h}{\bar{m}}$:

$$\Gamma = \oint \mathbf{v} \cdot d\mathbf{l} = \frac{\hbar}{\bar{m}} 2\pi\ell = \ell\frac{h}{\bar{m}}. \tag{36}$$

This implies that for a distance r from the center, the azimuthal velocity is

$$v_\theta = \ell\frac{\hbar}{\bar{m}r}. \tag{37}$$

If $\ell \neq 0$, the field must vanish when $r \to 0$. Otherwise, the kinetic energy due to this velocity would diverge. This structure will in fact define a vortex. As long as we have a field varying as $e^{i\ell\theta}$, its phase will wind from 0 to $2\pi\,|\ell|$ times. The vanishing intensity accounts for the undefined phase in the center. We call such a structure a vortex of charge ℓ. We define a single charge vortex for $|\ell| = 1$ and a multi-charge vortex for $|\ell| > 1$.

12

In this thesis we will always define the vortex field by $\psi_v(r,\theta) = \frac{r}{\sqrt{r^2+(\frac{\xi}{0.83})^2}}e^{i\ell\theta}$ [19]. We can see in Fig. 5 characteristics of such a vortex. It is also worth to mention that the healing length is the characteristic distance over which the fluid's order parameter recovers from the density going to zero at the core of a vortex. It sets the size of the vortex core. Except stated otherwise, we will use vortices of size $\xi = 17 \times 10^{-6}m$.
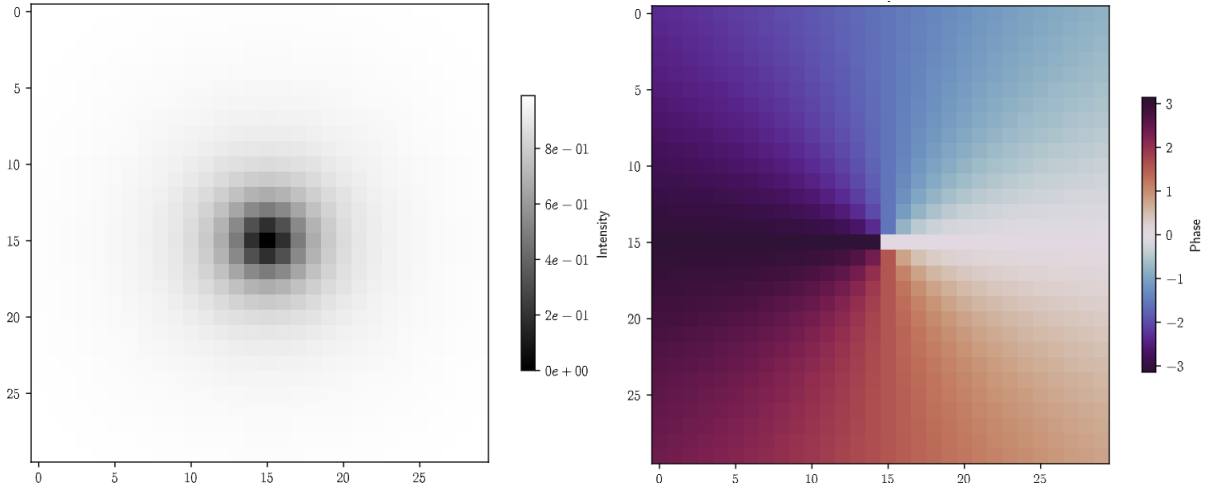
Figure 5: Intensity and phase of a single charge vortex. The intensity at the core of the vortex is null and recovers after the healing length which covers almost 2 pixels of size $p = 9.7 \times 10^{-6}m$, $\xi = 17 \times 10^{-6}m \approx 2p$ as expected. The phase winds from 0 to 2π once ($\ell = 1$).

In fact, as done in Ref. [19], it can be shown that a configuration with a multi-charge vortex of charge n is more energetic than a configuration with n single-charge vortices. This means that a multi-charge vortex would tend to dissipate its energy and split into multiple single-charge vortices. This effect will be of particular interest in the following Subsections.

3.2 Numerical Tool: Decomposition into Bogoliubov Modes in Spherical Coordinates

As we will detail in the following subsections, looking into vortex dynamics might involve looking into Bogoliubov modes. We are for example interested to see which modes might be emitted in the dissipation of energy when a multi-charged vortex splits. For this reason, a tool based on the NLSE Solver to decompose into these modes is necessary. We have seen that a vortex field goes as $e^{i\ell\theta}$. If we are also interested to look into modes labeled by their orbital angular momentum (OAM), it is interesting to work in the spherical $(r, \phi = \pi/2, \theta)$ basis[3] if we define the origin at the center of the plane of interest. We have also seen that after running the NLSE Solver (see Subsection 2.2), we can get 2D array for fixed positions z (in practice, we store this in 3D arrays where the third dimension corresponds to the z positions of interest). These arrays are however given in cartesian coordinates. For this reason, in order to look into the $e^{im\theta}$ modes, labeled by m we need to use the following algorithm:

---

[3]Looking at Fig. 1, if we define a spherical coordinates system for a fixed plane with azimuthal angle θ and polar angle ϕ, we would always be at $\phi = \pi/2$. For convenience, from now on, we will drop the $\pi/2$ from the notation.

- Project the array from the cartesian (x, y) basis onto the polar r, θ basis. *We now get a 2D array where the columns are given by θ and the rows by r.*[4]

- Perform a 1D Fourier transform along θ. *We now get a 2D array where the columns are given by m (conjugate variable to θ) and the rows by r.*[5]

- Look at the wanted observables. *The most useful observable in such cases where we need to know which modes are favored is usually the intensity*

Given this method, we can then get plots such as the one represented in Fig 6. As see in the figure, if we inject at the input vortices of charge ℓ, we expect to see a high intensity in the mode labeled by $m = \ell$, due to the structure of a vortex.
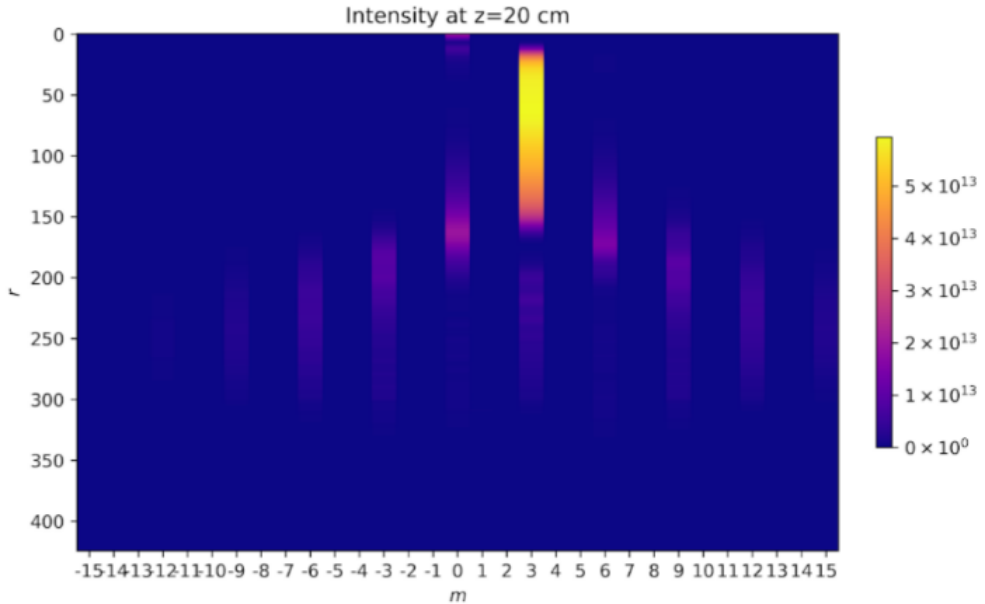
Figure 6: Intensity decomposition into spherical Bogoliubov modes for an input field $\psi \propto 0.9\psi_v + 0.1e^{iky}$, with the vortex being chosen of charge $l = 3$ and $k = 8.43m^{-1}$. Such a plot can be used for a spectral analysis, useful in cases such as the study of superradiance.

In Appendix A, we show how this decomposition can be used for the study of superradiance (which justifies the choice of the input $\psi \propto 0.9\psi_v + 0.1e^{iky}$) for example.

---

[4]It is important to know that as we are working with pixelized arrays, projecting into polar coordinates is not direct. For example, in cartesian coordinates, we can define the intensity as $\int I(x,y)dxdy$. In the polar case, we need to look, in a.u. at $\int I(r)rdr$. The method, inspired from https://stackoverflow.com/questions/3798333/image-information-along-a-polar-coordinate-system allows in fact to retrieve the r grid and thus, after squaring the electric field amplitude, we can just multiply by the r grid values and sum over the axis to get the total intensity in one mode. We also note that we are working in a discrete case so any integral transforms into a sum.

[5]In practice, numerical methods for a Fourier transform such as numpy.fft or cupy.fft give the positive frequencies then the positive ones. For better visualization, in the actual implementation we switch blocks of the array to get the mode for $m = 0$ at the center.

3.3 Stimulated and Spontaneous Dynamics

Vortices can be driven to behave following certain dynamics, we call such cases **stimulated dynamics**. An example of stimulated dynamics would be sending a perturbation (e.g e^{iky}, $e^{im\theta}$, etc.) that interacts with a vortex. These waves, scattering off the vortex can possibly extract energy from it and be amplified. In this energy extraction process, a multi-charge vortex can split to dissipate its energy. For a single charge vortex, it is still not clear theoretically how energy dissipates, but we will see shortly that we can still observe what we believe is an amplification (for a full rigorous study, quenches, which also are perturbations in the form of Bogoliubov modes should be eliminated as they could possibly be mistaken for amplification). Superradiance (see Appendix A) can be thought of as a stimulated process.

We can also have **spontaneous dynamics** occuring, especially with quantum noise. In the NLSE package, quantum noise could be possibly modeled classically using the method explained in Ref. [20]. For now, if needed, we just add random Gaussian noise.
Considering all of the above, it is interesting to study at which levels and frequencies of noise (quantum or classical), and at which rate (e.g. at which z do we see vortices splitting), can these dynamics happen.

A relevant analogy can be made with stimulated and spontaneous emission for atoms where spontaneous emission is driven by vacuum fluctuations whereas stimulated emission depends on the field we send.
To study stimulated processes, sending a plane wave perturbation is a good starting point as it can be decomposed into a superposition of many Bogoliubov modes.
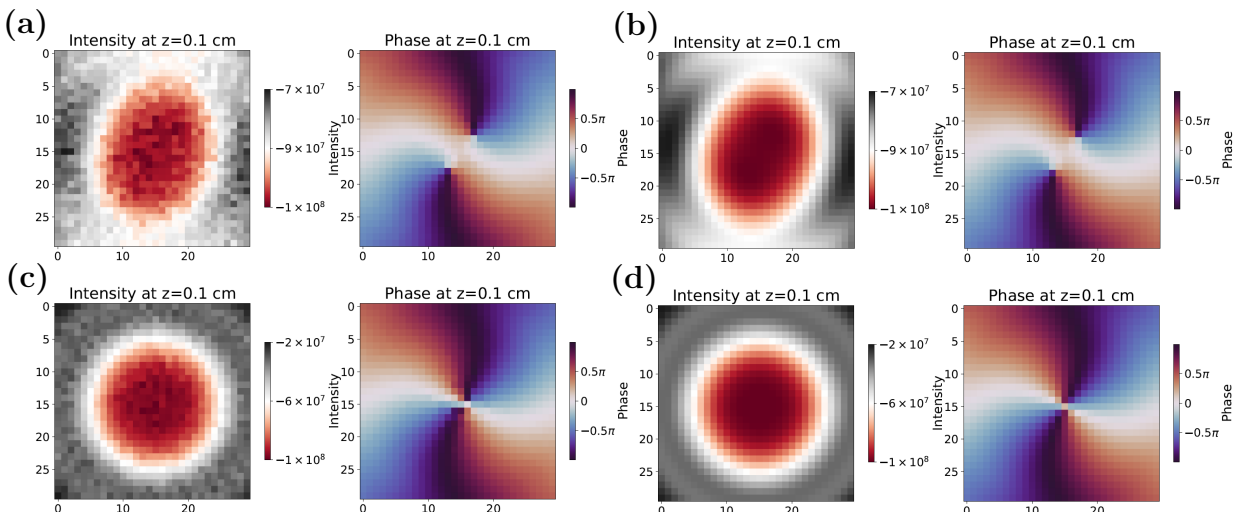
Figure 7: **(a)-(b)** Stimulated dynamics at $z = 0.1cm$. We send an input vortex field with a perturbation on top of the background of the form $\psi \propto 0.9\psi_v + 0.1e^{iky}$, $k = 100m^{-1}$. **(c)-(d)** Spontaneous Dynamics at $z = 0.1cm$ with $\psi = \psi_v$. For the left hand side simulations, gaussian random noise is added with an amplitude of 1% compared to the input field. **(b)-(d)** No Gaussian noise is added. For all simulations, the vortices are of charge $\ell = 2$ and healing length $\xi = 17 \times 10^{-6}m^{-1}$. The background intensity is also subtracted in all simulations.

In the following analysis, we will consider vortices to have split in the case where there is at least two pixels of separation in the phase.

We see from Fig. 7 that indeed, looking at the phase, when we send a perturbation, the vortices split rapidly (at least at $z = 0.1cm$ only). However, if we wait for spontaneous dynamics in the current model that we implement, it is difficult to observe with certainty the splitting of vortices even at $z = 15cm$ (see Fig. 8).
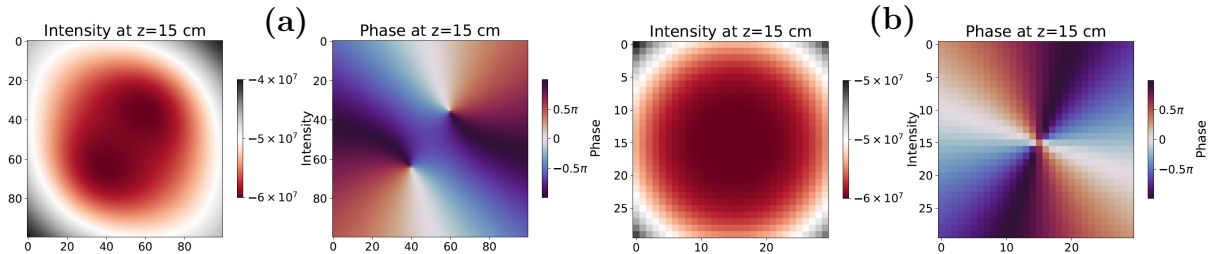
Figure 8: **(a)** Stimulated dynamics at $z = 15cm$. We send an input vortex field with a perturbation on top of the background of the form $\psi \propto 0.9\psi_v + 0.1e^{iky}$, $k = 100m^{-1}$. **(b)** Spontaneous Dynamics at $z = 15cm$ with $\psi = \psi_v$. For the left hand side simulations. For all simulations, no Gaussian noise is added, the vortices are of charge $\ell = 2$ and healing length $\xi = 17 \times 10^{-6}m^{-1}$. The background intensity is also subtracted.

But if we wait long enough, we can see at $z = 65cm$ (which is difficult to realize experimentally for usual cells of size $20cm$ at maximum.), the splitting, even without Gaussian noise, just from spontaneous dynamics becomes clear. In fact, we can even start seeing it (less obviously) starting around $30cm$. This hints that at least theoretically, and using the model we have, we could possibly have spontaneous splitting of vortices.
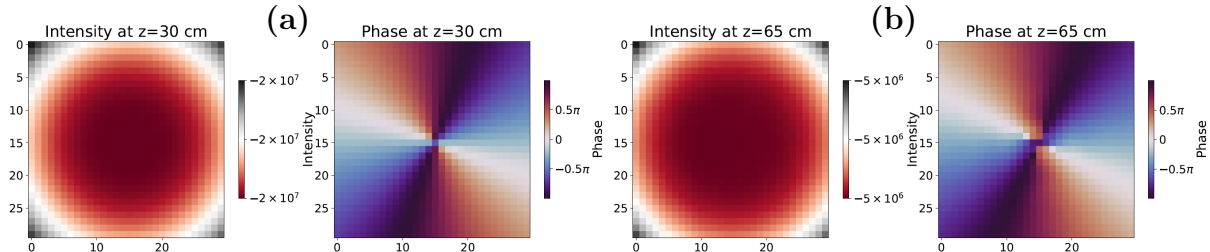
Figure 9: Spontaneous splitting of vortices at $z = 30cm$ **(a)** and $z = 65cm$ **(b)** with no noise or perturbation added. The parameters chosen are such that we chose an initial vortex with $\xi = 17 \times 10^{-6}$, $\ell = 2$. The simulation is done using $N = 4200$ pixels initially, that we crop to the center. Background intensity and phase is subtracted.

To get images as in Fig. 7, 8, or 9, increasing the number of pixels is necessary to be able to determine, looking at the phase, if the vortices split or not. However, this comes at the expense of computational time. In the figures above, we use at least 4200 pixels for the default window and then we zoom. An alternative approach, where the absorbing boundary conditions method might come into play would be to take a smaller window with less pixels (or take a smaller window). An interesting implementation for the future would be to automatize the code to see if vortices split or not, by looking at the phase. This would allow an enhanced study where we can rapidly test the change of many parameters such as effective propagation time z, charge ℓ, healing length ξ, perturbation amplitude, perturbation frequency k and noise amplitude.

We will now focus mainly on stimulated dynamics. As explained earlier, waves scattering off a vortex can be amplified by extracting energy from the vortex. This phenomenon seems to happen for all the range of plane wave frequencies and vortex charges that were tried (over more than 5 orders of magnitude for the frequencies starting from $k = 1m^{-1}$). As we will see in Section 4, inputting a vortex on top of the background alone creates perturbations due to quenching (see left hand side of Fig.10). It is not always easy to know what comes from quenching and what comes from an amplification. Nevertheless, quenches have a characteristic rings-like shape. When we add a plane wave perturbation traveling along the y direction for a vortex of $\ell = 1$ or $\ell = 6$, we can see in both cases that an amplification zone can be observed.
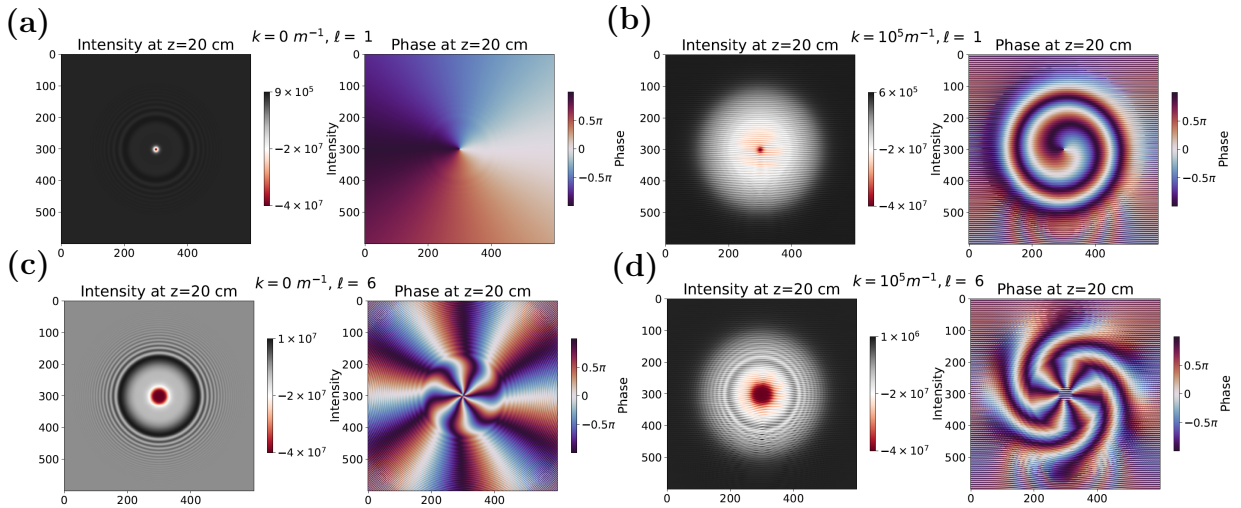
Figure 10: **(a)-(c)** Effect of injecting a vortex on top of the background with no noise or perturbation. Ring-like waves form due to quenching. **(b)-(d)** When a perturbation in the form of a plane wave with $k = 100000m^{-1}$ is added, its scattering off the vortex leads to an amplification. Vortices of charge $\ell = 1$ **(a)-(b)**, $\ell = 6$ **(c)-(d)** with the standard healing length were used. Background intensity and phase is subtracted.

We usually always have amplification zones, however, their direction and number seems to depend on the frequency of the plane wave injected as well as the initial vortex charge. As can be observed in Fig. 11, when a lower spatial frequency is used, the vortices, after splitting, reorganize in a specific way (which might be the most energetically favorable [6]) and then each vortex will create its own amplification zone. The more we propagate in effective time, the more the dark areas advance.

---

[6]An interesting phenomenon to study in such cases would be the movement of vortices. It could be possible that after this rearrangement, they stay stable.
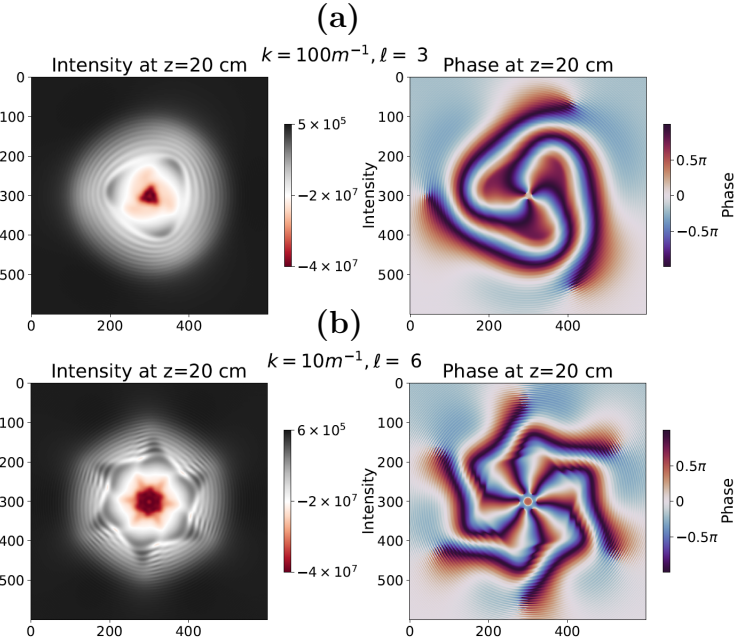
Figure 11: More examples of stimulated dynamics using plane waves of $k = 10m^{-1}$ **(a)** and $k = 100m^{-1}$ **(b)** and vortices of charges $\ell = 3$ **(a)** and $\ell = 6$ **(b)**. Background intensity and phase is subtracted.

Now that we have explored dynamics with plane wave perturbations, that we recall can be written as a superposition of the $e^{im\theta}$ modes[7], it is interesting to see how vortices interact if we inject such a mode only. Now, we define the input field on top of the background, as $\psi \propto 0.9\psi_v + 0.1e^{im\theta}$, with $\psi_v = f(r)e^{i\ell\theta}$.
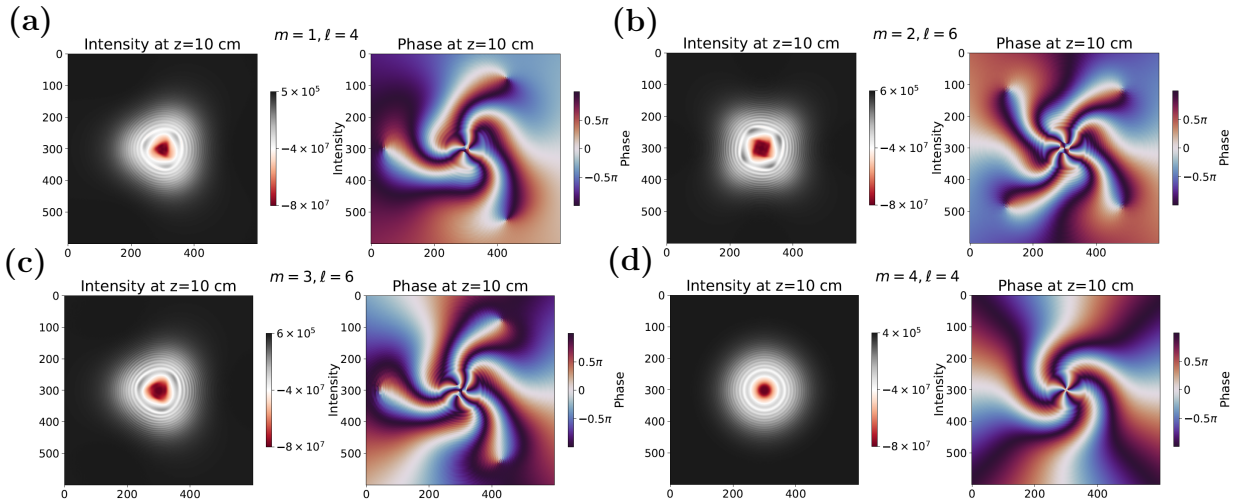
Figure 12: Input field on top of the background of the form $\psi \propto 0.9\psi_v + 0.1e^{im\theta}$. A pattern of $|m - l|$ amplification zones emerges. Background intensity and phase is subtracted.

---

[7]We will also sometimes call such modes m modes.

Using this perturbation, we see the emergence of $|m - l|$ zones of amplification. In the phase, we also observe $|m - l|$ points, other than the vortices, where the phase wraps from 0 to 2π. In the figure above, we tried perturbing with positive m modes only, however, this is equally possible with the use of $m < 0$ (see Fig. 13).
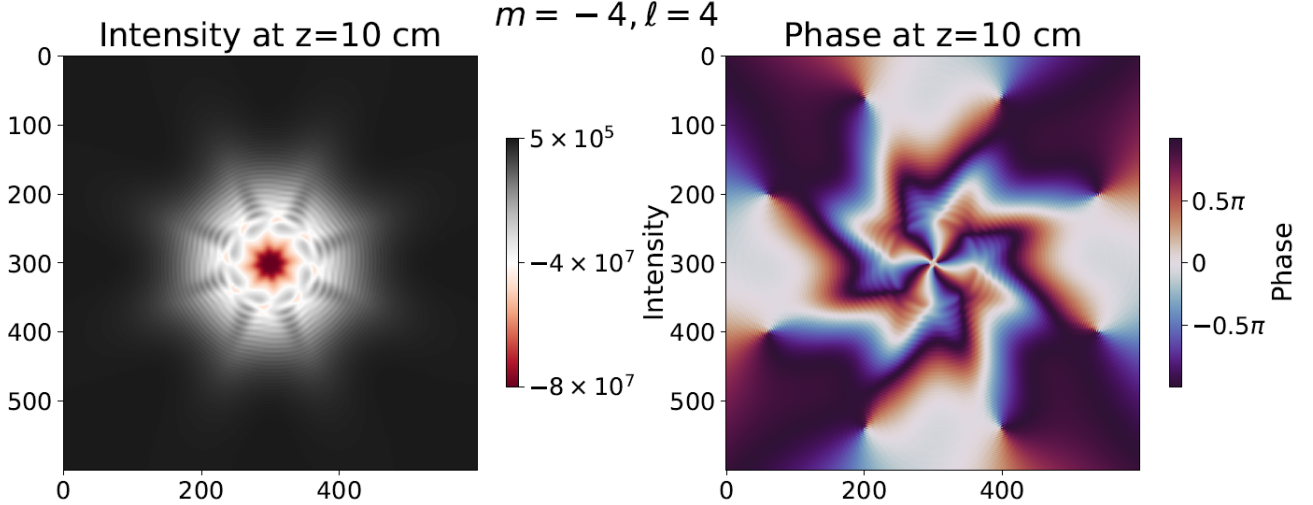
Figure 13: Input field on top of the background of the form $\psi \propto 0.9\psi_v + 0.1e^{im\theta}$ with $m = -4$ and $\ell = 4$ used. We see the emergence of 8 amplification zones.

An exact theoretical explanation has yet to be found. Mathematically, a possible direction for an explanation for the number of amplification zones could come from considering the interference patterns between all evolved waves and for which $\theta \in (0, 2\pi]$, possibly quantized by m, ℓ, we get bright fringes.

Looking at the intensity (integrated over all r as: $\int I(r)rdr$) evolution along z in the decomposition to modes m, we can get the following plots. As expected, we always have maximal intensity at $m = \ell$. When no perturbation is injected, we have a small intensity in other modes, due to quenches (which are difficult to discern without plotting in log scale, as their intensity is negligible). When a perturbation is injected, we can see that the intensity evolves in the modes, partly due to losses, but also because of the amplification. Some modes gain intensity while others lose in intensity at high times.
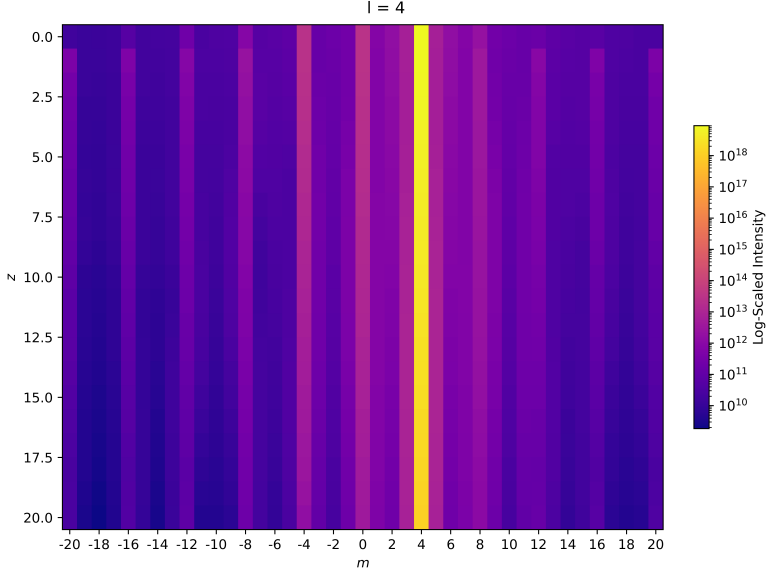
Figure 14: Log-scaled integrated intensity evolution in effective time for an input vortex of charge $\ell = 4$. Other perturbation modes can also be distinguished due to quenching. We crop to 40 m modes. z is in cm.
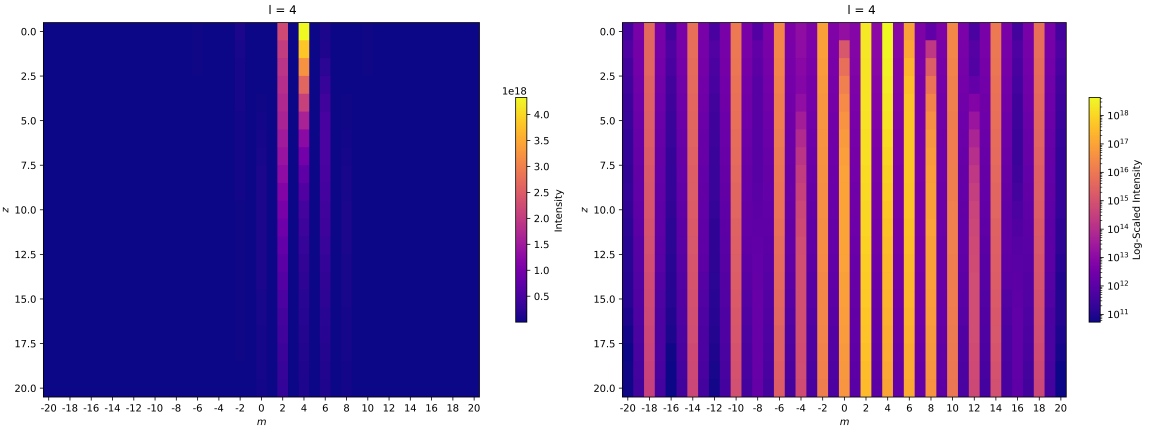
Figure 15: Integrated intensity (Left) and Log-scaled integrated intensity (Right) evolution in effective time for an input vortex of charge $\ell = 4$ with a perturbation in mode $m = 2$. Other perturbation modes can also be distinguished possibly due to quenching and amplification. We crop to 40 m modes. z is in cm.

4 Interaction Quenches

Out-of-equilibrium dynamics in quantum fluids of light refers to the behavior when the system does not settle into a stable state. One such example is when a parameter is suddenly changed. In paraxial fluids of light using hot atomic vapor cells, the geometry imposes this condition. Quenches come from the fact that interactions are suddenly turned on or off at the beginning or end of the cell. In this Section, we will study quenches closely. After modeling them, we will provide a possible observable that could characterize perturbations due to quenches. From one side, quenching is an important, well studied out-of-equilibrium phenomenon [21, 22, 23]. From the other side, it is interesting to try to eliminate it, in order to study vortex dynamics (and other) in equilibrium.

4.1 Origin of Quenching

In order to eliminate quenches, we first have to understand where do they come from and how can we model them. We will follow similar derivation steps as done in Ref. [8] and Murad Abuzarli's PhD thesis in Ref. [24].

In quantum fluids of light, unlike in Bose gases, photons effectively interact through their coupling with matter. Outside the cell, interactions are null. At the entrance of the cell, the system is directly driven out of equilibrium through the sudden change in interactions. The last term of the NLSE 10 reflects these interactions. To better understand this, suppose that for the input, we have a state centered at zero momentum. Nonlinear interactions could parametrically induce pairs of Bogoliubov excitations at $-k_\perp$ and $k_\perp$. At the end of the cell, after these excitations interfere, we pass again to a linear medium and the Bogoliubov excitations are transformed back to photons. In a more general sense, if the input is not an eigenmode of the system, the interaction quenches will yield the creation of Bogoliubov excitations. If we input a vortex field for example, we saw that perturbations with a characteristic ring-like pattern form (see Fig. 10). This phenomenon can be visualized as represented in Fig. 16.
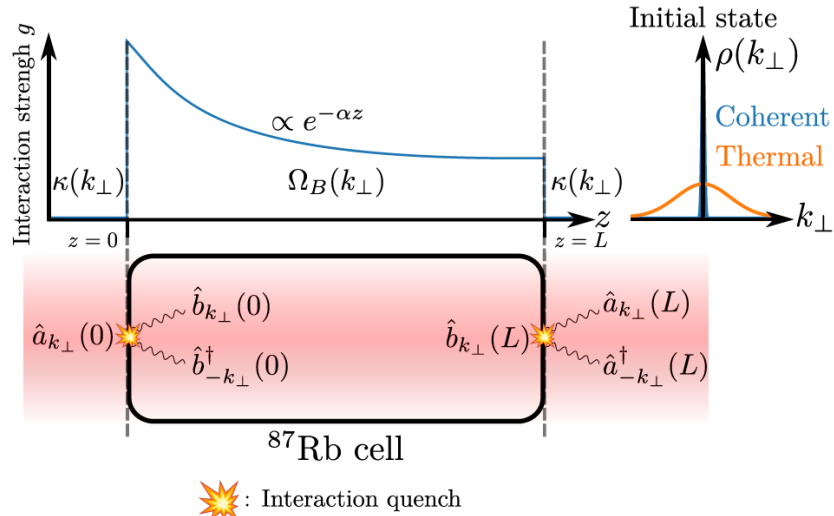
Figure 16: The creation of Bogoliubov excitations and their transformation back to photons is represented along the cell. The interactions sharply increase at the entrance of the cell and decrease at the end. Along the cell, absorption yields an exponential decay of these interactions. The curve on the right represents a possible initial state centered at zero momentum (blue) and final state (orange) with a characteristic distribution of thermal states. Image adapted from [8].

We already established in Section 2 that outside the medium, photon modes studied in k-space evolve, with dispersion relation $\kappa(\mathbf{k}_\perp) = \frac{\mathbf{k}_\perp^2}{2k_0}$ as:

$$\frac{\partial \hat{a}_{\mathbf{k}_\perp}}{\partial z} = i\frac{\mathbf{k}_\perp^2}{2k_0}(\mathbf{k}_\perp, z)\hat{a}_{\mathbf{k}_\perp},$$

$$\frac{\partial \hat{a}_{-\mathbf{k}_\perp}^\dagger}{\partial z} = -i\frac{\mathbf{k}_\perp^2}{2k_0}(\mathbf{k}_\perp, z)\hat{a}_{-\mathbf{k}_\perp}^\dagger. \tag{38}$$

Within the medium, perturbations (due to quenches for example) evolve as:

$$\frac{\partial \hat{b}_{\mathbf{k}_\perp}}{\partial z} = i\Omega_B(\mathbf{k}_\perp, z)\hat{b}_{\mathbf{k}_\perp},$$

$$\frac{\partial \hat{b}_{-\mathbf{k}_\perp}^\dagger}{\partial z} = -i\Omega_B^*(\mathbf{k}_\perp, z)\hat{b}_{-\mathbf{k}_\perp}^\dagger. \tag{39}$$

We also recall that the relation between a photon mode and a Bogoliubov mode is translated through the transformation:

$$\begin{pmatrix} \hat{a}_{\mathbf{k}_\perp}(z) \\ \hat{a}_{-\mathbf{k}_\perp}^\dagger(z) \end{pmatrix} = \begin{pmatrix} u_{\mathbf{k}_\perp}(z) & v_{\mathbf{k}_\perp}(z) \\ v_{\mathbf{k}_\perp}(z) & u_{\mathbf{k}_\perp}(z) \end{pmatrix} \begin{pmatrix} \hat{b}_{\mathbf{k}_\perp}(z) \\ \hat{b}_{-\mathbf{k}_\perp}^\dagger(z) \end{pmatrix}. \tag{40}$$

These evolution equations tells us that along z, the Bogoliubov excitations will pick up a phase that we denote by $\theta(\mathbf{k}_\perp, z) = \int_0^z \Omega_B(\mathbf{k}_\perp, z')dz'$. We will show that the Bogoliubov excitations possess correlations between the opposite momentum modes as they are produced simultaneously. The perturbations they can create can be studied rigorously using the static structure factor which translates the power of density fluctuations. It is also defined as the Fourier transform of the second order correlation function. If we use the hydrodynamic formulation in a second quantization language, considering a total number of particles N_0, the static structure factor is defined as:

$$S_{\mathbf{k}_\perp}(z) = \frac{1}{N_0} \left\langle \delta\hat{\rho}_{\mathbf{k}_\perp}^2(z) - |\langle \delta\hat{\rho}_{\mathbf{k}_\perp}(z)\rangle|^2 \right\rangle, \tag{41}$$

where the density fluctuation operator is $\delta\hat{\rho}_{\mathbf{k}_\perp}(z) = \int d\mathbf{q} \hat{a}_{\mathbf{k}_\perp+\mathbf{q}}^\dagger \hat{a}_{\mathbf{k}_\perp}$. Supposing the fluctuations are zero-mean, we get [25]:

$$S_{\mathbf{k}_\perp}(z) = \frac{1}{N_0} \langle \delta\hat{\rho}_{\mathbf{k}_\perp}(z)\delta\hat{\rho}_{-\mathbf{k}_\perp}(z)\rangle$$

$$= \frac{1}{N_0} \int d\mathbf{q}d\mathbf{q}' \left\langle \hat{a}_{\mathbf{q}-\mathbf{k}_\perp}^\dagger(z)\hat{a}_{\mathbf{q}}(z)\hat{a}_{\mathbf{q}'+\mathbf{k}_\perp}^\dagger(z)\hat{a}_{\mathbf{q}'}(z)\right\rangle. \tag{42}$$

Looking closely at this expression, one could understand the structure factor as an observable that could measure, by summing over all possible momenta, how many events transforming a mode from $\mathbf{q}$, $\mathbf{q}'$ to $\mathbf{q}-\mathbf{k}_\perp$, $\mathbf{q}'+\mathbf{k}_\perp$, while preserving conservation of momentum (in a nonlinear optics language, phase matching condition) happen. These events will thus reflect in some way how many photons and Bogoliubov modes are created and destroyed. We consider that for initial conditions, we have a coherent plane wave at zero momentum. If an initial condensate state is assumed to be at zero momentum, any scattering event that creates excitations necessarily at $-\mathbf{k}_\perp$ and $\mathbf{k}_\perp$ must be drawn from $\mathbf{q} = 0$ or $\mathbf{q}' = 0$. All the other contributions to the integral are null. This leaves us with:

$$S_{\mathbf{k}_\perp}(z) = \left\langle \hat{a}_{\mathbf{k}_\perp}^\dagger(z)\hat{a}_{\mathbf{k}_\perp}(z)\right\rangle + \left\langle \hat{a}_{\mathbf{k}_\perp}(z)\hat{a}_{\mathbf{k}_\perp}^\dagger(z)\right\rangle + \langle \hat{a}_{-\mathbf{k}_\perp}(z)\hat{a}_{\mathbf{k}_\perp}(z)\rangle + \left\langle \hat{a}_{\mathbf{k}_\perp}^\dagger(z)\hat{a}_{-\mathbf{k}_\perp}^\dagger(z)\right\rangle. \tag{43}$$

Using standard commutation relations for creation and annihilation operators, and defining photonic populations by $N_{\mathbf{k}_\perp}(z) = \left\langle \hat{a}^\dagger_{\mathbf{k}_\perp}(z)\hat{a}_{\mathbf{k}_\perp}(z) \right\rangle$ and photonic correlations by $C_{\mathbf{k}_\perp}(z) = \langle \hat{a}_{-\mathbf{k}_\perp}(z)\hat{a}_{\mathbf{k}_\perp}(z) \rangle$, we get:

$$S_{\mathbf{k}_\perp}(z) = 1 + 2N_{\mathbf{k}_\perp}(z) + 2\mathrm{Re}\left(C_{\mathbf{k}_\perp}(z)\right). \tag{44}$$

We consider first for simplicity that the population is fixed to N_0 inside the cell (outside the cell it is zero as no Bogoliubov excitations exist yet). This means that before the cell, $S_{\mathbf{k}_\perp}(z < 0) = 1$. At bigger effective times, we will start seeing oscillations around 1 as the modes will pick up a phase $\theta(z)$ making the last term proportional to $cos(\theta(z))$ while the second term stays constant; $S_{\mathbf{k}_\perp}(z > 0) = 1 + 2N_0 + 2C_0 cos(\theta(z))$. This is what makes the static structure factor a good observable to look at when considering quenches.

To study more exactly how will we get creation of pairs of Bogoliubov excitations starting with a vacuum state let us follow the reasoning below.
The assumptions that we made for the initial state at entrance of the cell ($z = 0$) read as:

$$N_{\mathbf{k}_\perp}(0) = \left\langle \hat{a}^\dagger_{\mathbf{k}_\perp}(0)\hat{a}_{\mathbf{k}_\perp}(0) \right\rangle = N_0\delta(\mathbf{k}_\perp)$$
$$C_{\mathbf{k}_\perp}(0) = \langle \hat{a}_{-\mathbf{k}_\perp}(0)\hat{a}_{\mathbf{k}_\perp}(0) \rangle = \delta(\mathbf{k}_\perp), \tag{45}$$

with vacuum in all $\mathbf{k}_\perp \neq 0$. We will now focus on these non-zero momentum modes as they are modes with the possibility to be excited due to quantum fluctuations. If we try to write the correlations and populations using the basis transformation, we will see that it is possible to have a non-zero population in a $\mathbf{k}_\perp \neq 0$ mode as soon as we are inside the cell:

$$\left\langle \hat{a}^\dagger_{\mathbf{k}_\perp}(0^+)\hat{a}_{\mathbf{k}_\perp}(0^+) \right\rangle = u_{\mathbf{k}_\perp}(0^+)v_{\mathbf{k}_\perp}(0^+) \left\langle \hat{b}_{-\mathbf{k}_\perp}(0^+)\hat{b}_{\mathbf{k}_\perp}(0^+) \right\rangle + v^2_{\mathbf{k}_\perp}(0^+) \left\langle \hat{b}_{-\mathbf{k}_\perp}(0^+)\hat{b}^\dagger_{-\mathbf{k}_\perp}(0^+) \right\rangle +$$
$$u^2_{\mathbf{k}_\perp}(0^+) \left\langle \hat{b}^\dagger_{\mathbf{k}_\perp}(0^+)\hat{b}_{\mathbf{k}_\perp}(0^+) \right\rangle + u_{\mathbf{k}_\perp}v_{\mathbf{k}_\perp} \left\langle \hat{b}^\dagger_{\mathbf{k}_\perp}(0^+)\hat{b}^\dagger_{-\mathbf{k}_\perp}(0^+) \right\rangle$$
$$\langle \hat{a}_{-\mathbf{k}_\perp}(0^+)\hat{a}_{\mathbf{k}_\perp}(0^+) \rangle = u^2_{\mathbf{k}_\perp}(0^+) \left\langle \hat{b}_{-\mathbf{k}_\perp}(0^+)\hat{b}_{\mathbf{k}_\perp}(0) \right\rangle + u_{\mathbf{k}_\perp}(0^+)v_{\mathbf{k}_\perp}(0^+) \left\langle \hat{b}_{-\mathbf{k}_\perp}(0^+)\hat{b}^\dagger_{-\mathbf{k}_\perp}(0^+) \right\rangle +$$
$$u_{\mathbf{k}_\perp}(0^+)v_{\mathbf{k}_\perp}(0^+) \left\langle \hat{b}^\dagger_{\mathbf{k}_\perp}(0^+)\hat{b}_{\mathbf{k}_\perp}(0^+) \right\rangle + v^2_{\mathbf{k}_\perp}(0^+) \left\langle \hat{b}^\dagger_{\mathbf{k}_\perp}(0^+)\hat{b}^\dagger_{-\mathbf{k}_\perp}(0^+) \right\rangle. \tag{46}$$

This further simplifies to:

$$\left\langle \hat{b}_{-\mathbf{k}_\perp}(0^+)\hat{b}_{\mathbf{k}_\perp}(0^+) \right\rangle = \left\langle \hat{b}^\dagger_{\mathbf{k}_\perp}(0^+)\hat{b}^\dagger_{-\mathbf{k}_\perp}(0^+) \right\rangle = -u_{\mathbf{k}_\perp}(0^+)v_{\mathbf{k}_\perp}(0^+)$$
$$\left\langle \hat{b}_{-\mathbf{k}_\perp}(0^+)\hat{b}^\dagger_{-\mathbf{k}_\perp}(0^+) \right\rangle = u^2_{\mathbf{k}_\perp}(0^+) \tag{47}$$
$$\left\langle \hat{b}^\dagger_{\mathbf{k}_\perp}(0^+)\hat{b}_{\mathbf{k}_\perp}(0^+) \right\rangle = v^2_{\mathbf{k}_\perp}(0^+).$$

In fact, if we pause and think about Eq. 47, we can already see that it is enough to have $v_{\mathbf{k}_\perp}(0^+) \neq 0$ to get a non zero number of Bogoliubov excitations (quasi-particles) in $\mathbf{k}_\perp$. In fact, this is true as long as we are in a medium with non-zero interactions. Rigorously, we can show, by solving system 29, that this is true as, for a dispersion $\Omega_B(\mathbf{k}_\perp) = \pm\sqrt{\frac{\mathbf{k}_\perp^2}{2k_0}\left(\frac{\mathbf{k}_\perp^2}{2k_0} + 2\bar{g}|\mathcal{E}_0|^2\right)} - i\frac{\alpha}{2}$:

$$u_{\mathbf{k}_\perp}(z), v_{\mathbf{k}_\perp}(z) = \frac{1}{2}\left[\left(\frac{2\Omega_B\bar{m}}{\hbar\mathbf{k}_\perp^2}\right)^{1/2} \pm \left(\frac{\hbar\mathbf{k}_\perp^2}{2\Omega_B\bar{m}}\right)^{1/2}\right]. \tag{48}$$

In a similar fashion, we can continue the analysis up to the end of the cell ($z = L$). From Eq. 39, we get considering losses:

$$\left\langle \hat{b}_{-\mathbf{k}_\perp}(L)\hat{b}_{\mathbf{k}_\perp}(L) \right\rangle = \left\langle \hat{b}_{\mathbf{k}_\perp}^\dagger(L)\hat{b}_{-\mathbf{k}_\perp}^\dagger(L) \right\rangle = -u_{\mathbf{k}_\perp}(L)v_{\mathbf{k}_\perp}(L)e^{2i\theta(L)}$$

$$\left\langle \hat{b}_{-\mathbf{k}_\perp}(L)\hat{b}_{-\mathbf{k}_\perp}^\dagger(L) \right\rangle = u_{\mathbf{k}_\perp}^2(L)e^{-\alpha L} \tag{49}$$

$$\left\langle \hat{b}_{\mathbf{k}_\perp}^\dagger(L)\hat{b}_{\mathbf{k}_\perp}(L) \right\rangle = v_{\mathbf{k}_\perp}^2(L)e^{-\alpha L}.$$

If we transform back to the photonic basis, we get:

$$\left\langle \hat{a}_{\mathbf{k}_\perp}^\dagger(L)\hat{a}_{\mathbf{k}_\perp}(L) \right\rangle = -u_{\mathbf{k}_\perp}(0^+)v_{\mathbf{k}_\perp}(0^+)u_{\mathbf{k}_\perp}(L)v_{\mathbf{k}_\perp}(L)\left[e^{-2i\theta(L)} + e^{2i\theta(L)}\right] +$$
$$v_{\mathbf{k}_\perp}^2(L)u_{\mathbf{k}_\perp}^2(0^+) + v_{\mathbf{k}_\perp}^2(0^+)u_{\mathbf{k}_\perp}^2(L)$$
$$\langle \hat{a}_{-\mathbf{k}_\perp}(L)\hat{a}_{\mathbf{k}_\perp}(L) \rangle = -u_{\mathbf{k}_\perp}(0^+)v_{\mathbf{k}_\perp}(0^+)u_{\mathbf{k}_\perp}(L)v_{\mathbf{k}_\perp}(L)\left[u_{\mathbf{k}_\perp}^2(L)e^{-2i\theta(L)} + v_{\mathbf{k}_\perp}^2(L)e^{2i\theta(L)}\right] +$$
$$u_{\mathbf{k}_\perp}(L)v_{\mathbf{k}_\perp}(L)\left[u_{\mathbf{k}_\perp}^2(0^+) + v_{\mathbf{k}_\perp}^2(0^+)\right]. \tag{50}$$

And for a step δ after the cell, we finally get a conserved photonic population and dephased correlations:

$$\left\langle \hat{a}_{\mathbf{k}_\perp}^\dagger(L+\delta)\hat{a}_{\mathbf{k}_\perp}(L+\delta) \right\rangle = \left\langle \hat{a}_{\mathbf{k}_\perp}^\dagger(L)\hat{a}_{\mathbf{k}_\perp}(L) \right\rangle$$

$$\langle \hat{a}_{-\mathbf{k}_\perp}(L+\delta)\hat{a}_{\mathbf{k}_\perp}(L+\delta) \rangle = e^{-2i\kappa\delta}\langle \hat{a}_{-\mathbf{k}_\perp}(L)\hat{a}_{\mathbf{k}_\perp}(L) \rangle. \tag{51}$$

As expected, at the end of the cell, we get complex populations and correlations coming from the different excitations that interfered along the cell.

4.2   Numerical Tool: A Possible Observable for Perturbations

We saw that to study quenches rigorously, we should look at the static structure factor observable or at the second order correlation function $g^{(2)}$. In this subsection, we also offer a fast numerical way to check roughly the perturbations coming from quenches. Suppose first that for the input field we inject a vortex ψ_v on top of the background ψ_0. Any perturbation created in the cell can possibly create oscillations in the intensity. Since we know that quenches create radially symmetric oscillations, we will consider for observable the density, on top of that of the background as a function of r, which we can measure numerically as: $\sqrt{I(r)} - \sqrt{I_0(r)}$ (after performing an azimuthal average over a specified region of the array). We note that numerically, we will not consider the quench at the end of the cell as we are imaging directly in the planes of interest. Hence, the more we proceed in effective time, the more the perturbations due to quench will dissipate until eventually disappearing.[8] This effect is depicted in Fig. 17. PhD student Myrann B. Rasooli checked that as theorized by Bogoliubov Theory, these perturbations travel in z at the speed of sound.

---

[8]This is true if we include or not losses in the simulations.
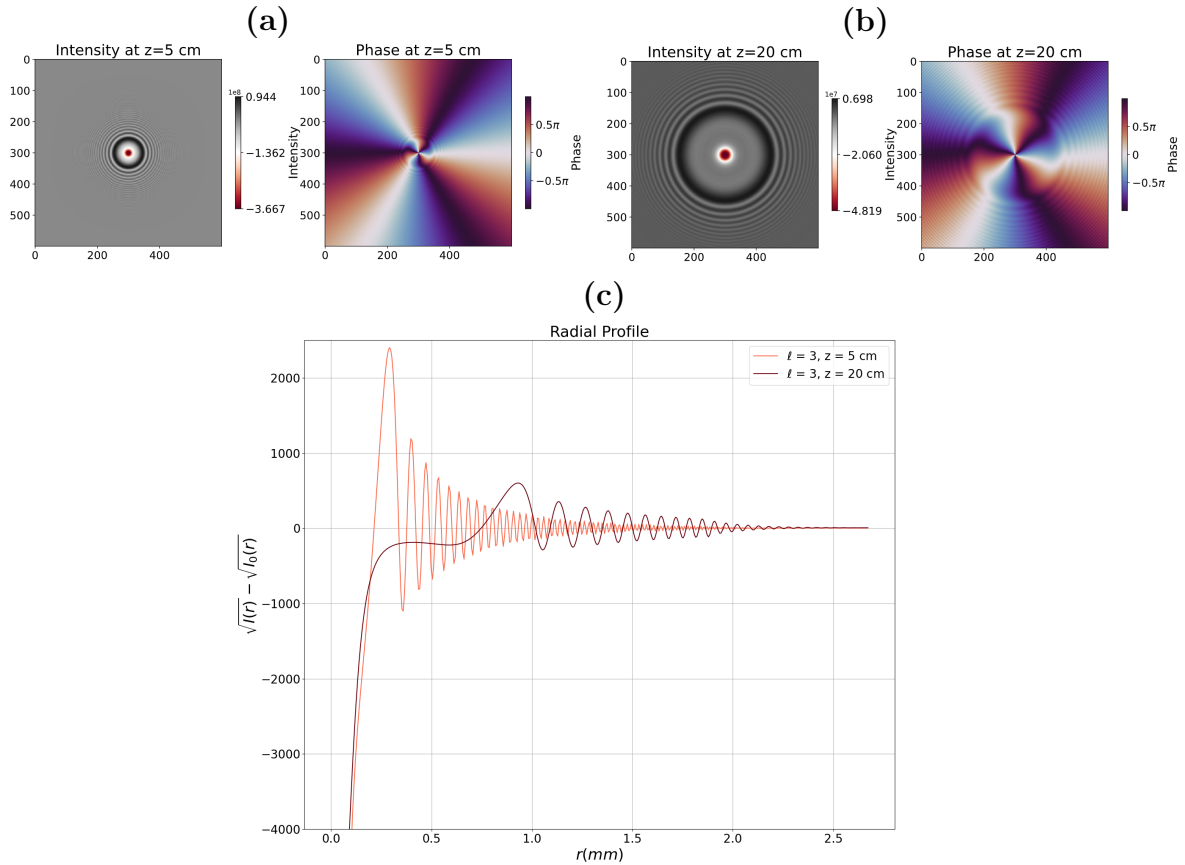
Figure 17: Intensity and phase (background is subtracted) for input vortex of charge $\ell = 3$ at $z = 5cm$ (a) and $z = 20cm$ (b). The perturbations due to quench dissipate along the cell. (c) Radial profile $\sqrt{I(r)} - \sqrt{I_0(r)}$ showing perturbations attenuated at high effective time.

4.3 Numerical Post-Processing

In principle, if one wants to exclude the effects of quenches from the data analysis, we could think about ways either to eliminate it since the entrance of the cell, or by using image analysis techniques. In this Subsection, we will explain the latter. To do this, we will first suppose that for the same input vortex, the consequent perturbations happen in the same way all the time. We also assume that the vortex field doesn't change a lot along the cell. We consider every perturbation on top of the vortex and the background to come from quenching. Hence, if we first run a simulation for an input of only a vortex on top of the background, we can retrieve the perturbations, by taking the difference with the ideal case being the vortex and background only. For each fixed z, we hence save $\Delta E = E - E_{ideal} = E - E_0 \times \psi_v$.

The last step would then only be to subtract the saved perturbations ΔE (which is an array) from the NLSE-simulated array at each step. This can also be done for simulations with different inputs. If the input has an extra plane wave, we also include it in the ideal field, etc. To be more explicit, if we take for example Fig. 10, we track the perturbations from (a) and try to remove them when simulating (b). In Fig. 18, we run a simulation when the quenching effect is removed using this technique. It shows clearly that the ring-like perturbations don't exist anymore using such a method.
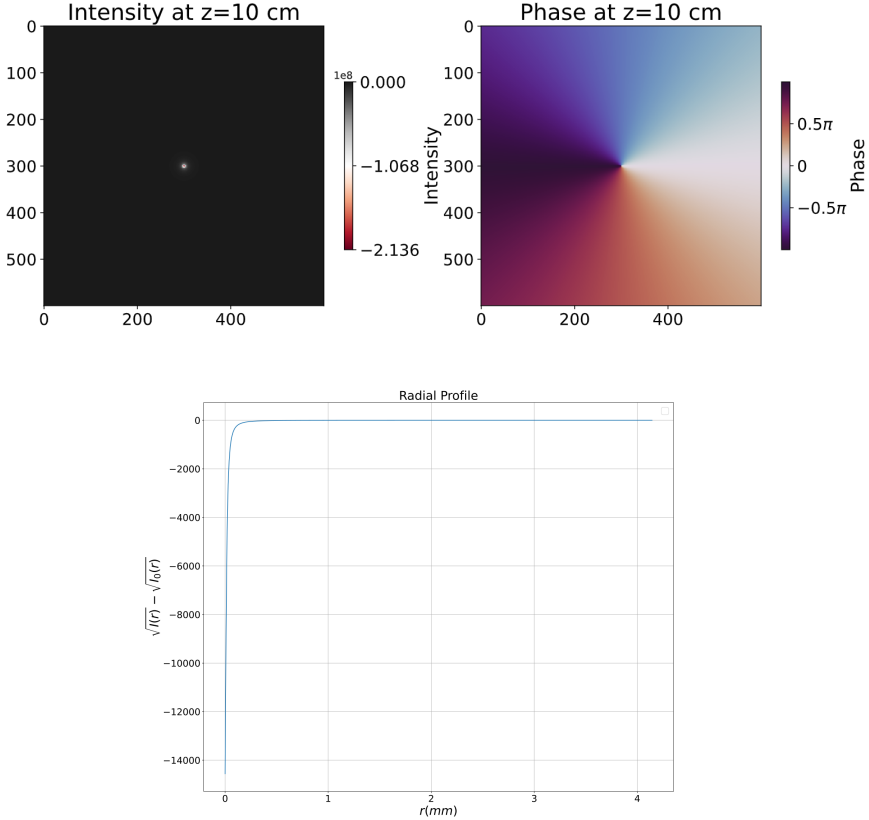
Figure 18: Simulation after removing the quenching effect at $z = 10cm$. The ring-like pattern disappears. After tracking the perturbations and saving them in an initial simulation, we remove them from the images in the new run. The radial profile is also shown on the right: no perturbations are present.

This method is limited. It is a post-processing method that eliminates quenches from the analysis. Their effects in the intrinsic simulations are nevertheless always present. We just remove extra perturbations by comparing to the ideal case and this doesn't eliminate the quenching effect on vortex dynamics. It can be seen as a method to remove the quenches from the images and plots (which still affects intensity and phase readings) but not from the intrinsic dynamics.

4.4   Antiquenching

The method explained in Subsection 4.3 above has obvious limits. From an experimental point of view, it is impossible to get the same conditions at the same z every time, making it difficult to use this method to calibrate by the perturbations. We thus need to explore options that are more experimentally feasible. In this Subsection, we will study two of them. While the first one is also not very easy to realize, the second one might be the most promising for a paraxial fluids of light system. The results shown in this Subsection are still preliminary and further effort can be put in that regard.

4.4.1   Numerical Tool: Ramping Interactions Adiabatically

We saw that quenches in our system come from the fact that interactions are suddenly turned on and off at the cell boundaries. In simulations, we could possible overturn this by trying to adiabatically change the non-linearity (that we control by n_2) along z. In

simulations, this can be easily achieved using a callback function that internally changes the value associated to n_2 after each simulation step. We define any function that we want while making sure that $n_2(0) = 0$.

In a first trial (see Fig. 19), we could see that different rampings for $n_2(z)$ could possibly affect the perturbations in the radial profile.
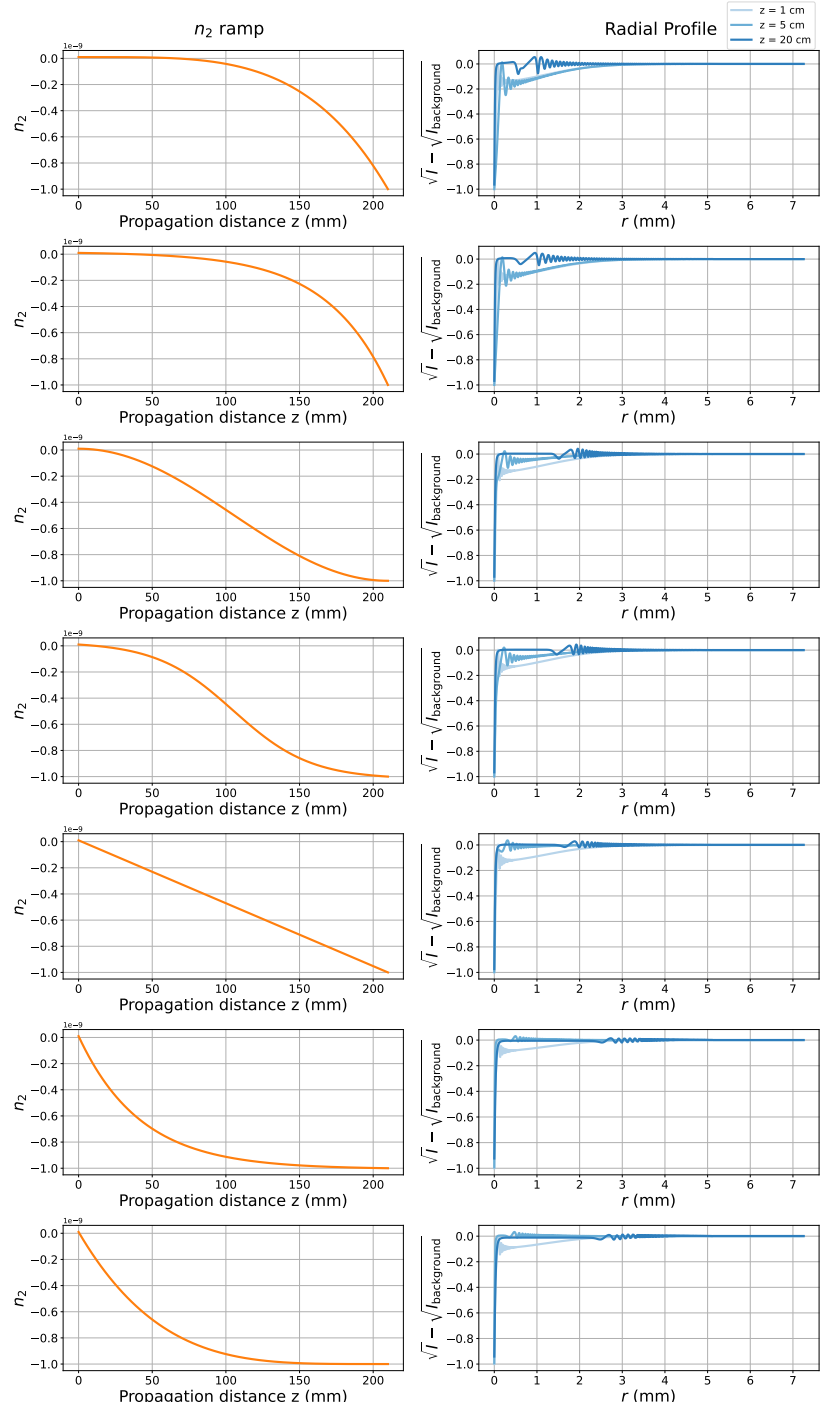
Figure 19: Radial profiles for different ramps with fixed $n_2(0) = 0m^2/W$ and $n_2(z = 210mm) = -10^{-9}m^2/W$. The perturbations seem to soften and dissipate faster for the last few ramps, however, this only comes from the fact that the overall experienced interactions are lower. I and $I_{backround}$ are normalized before taking the difference of square roots. A vortex of charge $\ell = 1$ and $\xi = 10^{-5}m$ is used.

27

However, the correct interpretation in that specific case is not that the adiabatic changes are leading to lower perturbations. The effect only comes from the fact that we are going from high to low overall interactions. In other terms the integral under the curve of n_2 is not fixed in Fig. 19. To rigorously study the effect, we thus have to choose parametrizations for the ramp [9] that conserve the integral under the curve as done in Fig. 20. Even using this method, quenches were not eliminated. Trying to ramp only between $z = 0$ and $z = z' < L$, then keeping the interactions constant didn't eliminate the quench too. Ideally, we would like to find a ramp that reduces the quenching effect for all z while keeping the highest non-linearity possible in a low-losses regime.

4.4.2 Injection of Antiquenches with a Vortex

One might think that a good strategy would be to get the perturbations (defined as any contribution to the electric field on top of the input) very close to $z = 0$ and then, add the π phase-shifted corresponding field to the input, in the hope that they will directly interfere destructively and disappear. However, this strategy isn't optimal in our system as we are dealing with a nonlinear medium where the superposition principle doesn't apply. It has been tried for different vortex sizes and different simulation parameters without a lot of improvement. A better strategy would thus be to study the perturbations in the Bogoliubov transformed basis, using Eq. 40 as well as 48 before injecting them. Such a strategy would be based on looking into the Bogoliubov modes early inside the cell, in a first simulation and then transforming them to photonic modes that are injected as antiquenches by adding them to the vortex field in another simulation.

---

[9]The functions used can be found on the github.
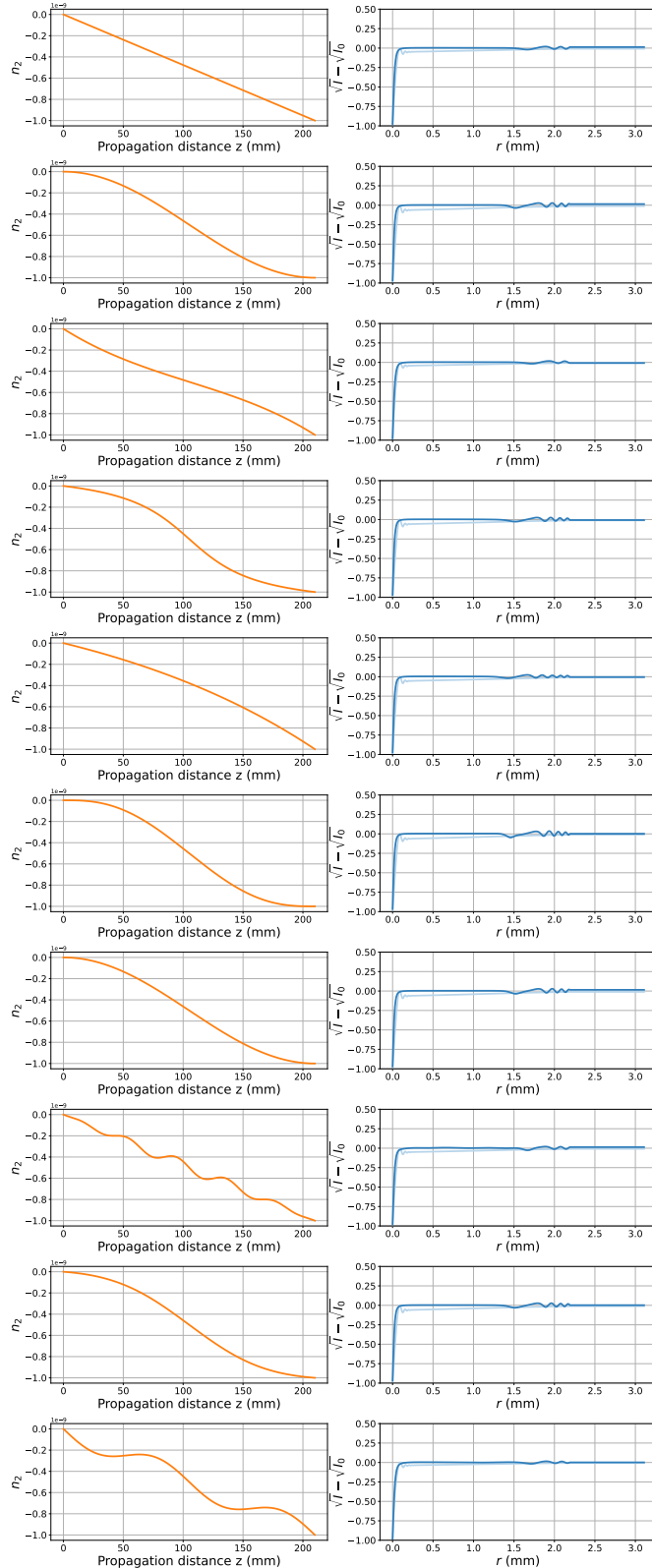
Figure 20: Radial profiles for different ramps with fixed $n_2(0) = 0m^2/W$ and $n_2(z = 210mm) = -10^{-9}m^2/W$ with fixed integral under the curve. The perturbations in that case follow almost the same pattern for all ramps. In no case quenches were fully eliminated. I and I_0 are normalized before taking the difference of square roots. A vortex of charge $\ell = 1$ and $\xi = 17 \times 10^{-6}m$ is used.

29

5 Conclusion and Future Work

Throughout this thesis, we explored how paraxial fluids of light provide a great platform to test ultracold physics phenomena with a simple, highly-controllable setup. The mapping between the NLSE and the GPE is the basis for bridging the gap between non-linear optics and many body physics.

We have seen how spontaneous and stimulated vortex dynamics could occur in such systems. Waves scattering off a vortex can amplify, multi-charged vortices can split, etc. Theoretical as well as practical effort can still be made in that regard in order to better understand how energy dissipates, the role of quantum fluctuations in these dynamics, and their accurate inclusion in simulations.

The geometry of paraxial fluids of light imposes for now the study of effects out of equilibrium, due to interaction quenches at the start and end of the cell. We have strategies to remove them from the analysis but effort can still be made to study dynamics in a regime at equilibrium by antiquenching.

Appendix

A   Superradiance

Superradiance is a phenomenon common to many fields of physics. We study it in the context of waves scattering off a vortex. It has been observed in water bathtub experiments [26] as well as in quantum fluids of light [27]. A lot of the existing literature uses analog gravity language to describe it (superradiance can be seen from the point of view of a stimulated Hawking effect). In this Appendix, we will provide an analysis comparable to that of the existing literature. We can also use this to test the tools we developed. However, by essence, the explanation is the same as the amplification process explained in Section 3.

A.1   Theoretical Background

As explained in Ref. [26], a wave ζ (e.g. a plane wave) can be decomposed into partial waves as:

$$\zeta(\bar{t}, r, \theta) = \mathrm{Re}\left[\sum_{m\in\mathbb{Z}} \int_0^\infty \varphi_{\bar{f},m}(r) \frac{\mathrm{e}^{-2i\pi\bar{f}\bar{t}+im\theta}}{\sqrt{r}}\mathrm{d}\bar{f}\right] = \mathrm{Re}\left[\sum_{m\in\mathbb{Z}} \int_0^\infty \Phi_{k_0,m}(r) \frac{\mathrm{e}^{-ik_0 z+im\theta}}{\sqrt{r}}\mathrm{d}k_0\right].$$
(52)

We also define, for each partial wave, an effective frequency $\bar{\omega} = 2\pi\bar{f}$. In the fluid's reference frame rotating at $\Omega(r) = \frac{v_\theta}{r} = \frac{\hbar\ell}{\bar{m}r^2}$ (this holds true if $v_r \ll v_\theta$, otherwise, this expression is more complex), $\bar{\omega}$ is perceived, due to the Doppler effect as [10]

$$\omega_{fluid}(r) = \bar{\omega} - m\Omega(r) = \bar{\omega} - \mathbf{k}_\theta(r).\mathbf{v}(r),$$
(53)

where $k_\theta = \frac{m}{r}$.[11] It can be shown that to have superradiance, for some region we need to have negative perceived frequencies yielding the condition

$$\bar{\omega} < m\Omega.$$
(54)

When such negative frequency partial waves interact with the vortex inside what we call the ergoregion, due to conservation of energy, an amplification of energy should be observed for the reflected waves scattering off the vortex. We think that this interaction could induce the splitting of vortices, for energy to be conserved. In simple terms, the vortex "wins negative energy", while the waves are "losing negative energy".

If we define $m' := m - l$, it can be shown that the superradiance condition is equivalent to having the intensity in the $-m'$ mode higher than the intensity in the m' mode [27], [28]. Looking at Fig. 6, this means that if we fix a region in r and look at columns symmetric with respect to l, we should see a brighter intensity on the left than on the right.

---

[10]This can be trivially seen since $\theta_{fluid} = \theta - \Omega\bar{t}$, $e^{-i\bar{\omega}\bar{t}+im\theta} = e^{-i\bar{\omega}\bar{t}+im(\theta_{fluid}+\Omega\bar{t})} = e^{-i(\bar{\omega}-m\Omega)\bar{t}+im\theta_{fluid}}$

[11]The azimuthal wave number m is not to be confused with effective mass $\bar{m}$.

A.2   Numerical Tool: Ergoregion Calculation

In order to make a full analysis, when we look at superradiance, we should be able to find the ergoregion around a vortex.[12] In quantum fluids of light, the ergoregion is defined by the critical radius r_e at which $v(r) = c_s(r)$ [13]. Usually, the tangential flow v_θ is the most significant part of the velocity so we write $v(r) \approx v_\theta(r)$. This condition means that for radii where $v_\theta(r) < c_s$, waves can travel against the flow. When $v_\theta(r) > c_s$, the flow speed overtakes the wave speed, and the region becomes an ergoregion. This means that within the ergoregion, any excitation is dragged along by the fluid.

We recall that $c_s(r) = c\sqrt{n_2 I(r)}$. Within the NLSE solver 2.2, a code for finding the radial and tangential velocity components was also developed. Using numpy.where or cupy.where, it then becomes numerically easy to find the crossings between speed of sound and tangential velocity. Sometimes, numerically, we get a function for v_θ that increases rapidly for small r and then decreases, yielding 2 intersection points (which are usually approximately equal), we take by default the biggest. For multi-charge vortices, we consider one effective ergoregion also by taking the biggest intersection point.

After finding the ergoregion r_e, we can then plot the difference in intensities between the m' and $-m'$ modes that we define respectively by $u_{m'}^2$ and $v_{m'}^2$ as a function of r. If we send a plane wave perturbation, we get for different plane wave frequencies k, ℓ and z the characteristic superradiance plot as in Fig. 21. Quenching might affect the analysis. However, we can see the signature where inside the ergoregion, the intensity in the negative modes, trapped near the vortex, is higher than the positive ones.
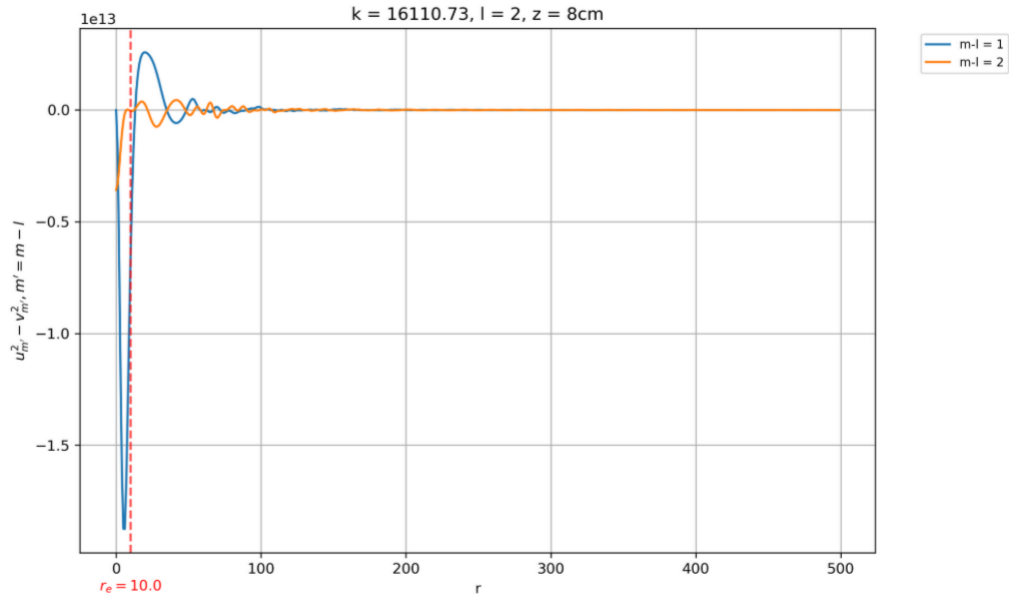
Figure 21: Difference between intensities $u_{m'}^2$ (in m' mode) and $v_{m'}^2$ (in $-m'$ mode) as a function of r. We represent by a dashed line the ergoregion r_e. Within this ergoregion, we have a higher intensity in negative modes. The ergoregion is at $r_e = 10p \approx 10^{-4}m = 0.1mm$, with p pixel size. We use a plane wave perturbation with $k = 16110.73m^{-1}$, $\ell = 2$, and look at $z = 8cm$.

---

[12]The name is similar to the one used in black hole physics where the ergoregion of a rotating black hole is where no static observers can remain at rest because the spacetime is dragged by the rotation.

[13]We will consider azimuthal averages over θ.

References

[1] J. Dalibard and C. Cohen-Tannoudji. "Laser cooling below the Doppler limit by polarization gradients: simple theoretical models". In: *J. Opt. Soc. Am. B* 6.11 (Nov. 1989), pp. 2023–2045. DOI: `10.1364/JOSAB.6.002023`.

[2] Steven Chu et al. "Experimental Observation of Optically Trapped Atoms". In: *Phys. Rev. Lett.* 57 (3 July 1986), pp. 314–317. DOI: `10.1103/PhysRevLett.57.314`.

[3] William D. Phillips and Harold Metcalf. "Laser Deceleration of an Atomic Beam". In: *Phys. Rev. Lett.* 48 (9 Mar. 1982), pp. 596–599. DOI: `10.1103/PhysRevLett.48.596`.

[4] A. Einstein. "Quantentheorie des einatomigen idealen Gases". In: *Albert Einstein: Akademie-Vorträge.* John Wiley Sons, Ltd, 2005, pp. 237–244. ISBN: 9783527608959. DOI: `https://doi.org/10.1002/3527608958.ch27`.

[5] M. H. Anderson et al. "Observation of Bose-Einstein Condensation in a Dilute Atomic Vapor". In: *Science* 269.5221 (1995), pp. 198–201. DOI: `10.1126/science.269.5221.198`.

[6] E. P. Gross. "Structure of a quantized vortex in boson systems". In: *Nuovo Cim* 20 (May 1961), pp. 454–477. DOI: `https://doi.org/10.1007/BF02731494`.

[7] L. P. Pitaevskii. "Vortex Lines in an Imperfect Bose Gas". In: *Soviet Physics JETP* 13.2 (1961), pp. 451–454.

[8] Tangui Aladjidi. "Full optical control of quantum fluids of light in hot atomic vapors". 2023SORUS406. PhD thesis. 2023. URL: `http://www.theses.fr/2023SORUS406/document`.

[9] T. Aladjidi Q. Glorieux C. Piekarski. "Paraxial fluids of light". not yet published.

[10] Robert W. Boyd. *Nonlinear Optics.* 3rd. Academic Press, 2008.

[11] Quentin Fontaine et al. "Interferences between Bogoliubov excitations in superfluids of light". In: *Phys. Rev. Res.* 2 (4 Dec. 2020), p. 043297. DOI: `10.1103/PhysRevResearch.2.043297`.

[12] Tangui Aladjidi, Clara Piekarski, and Quentin Glorieux. "NLSE: A Python package to solve the nonlinear Schrödinger equation". In: *Journal of Open Source Software* 9.99 (2024), p. 6607. DOI: `10.21105/joss.06607`.

[13] E. Madelung. "Eine anschauliche Deutung der Gleichung von Schrödinger". In: *Naturwissenschaften* 14.45 (1926), pp. 1004–1004. DOI: `https://doi.org/10.1007/BF01504657`.

[14] Pierre-Élie Larré and Iacopo Carusotto. "Propagation of a quantum fluid of light in a cavityless nonlinear optical medium: General theory and response to quantum quenches". In: *Phys. Rev. A* 92 (4 Oct. 2015), p. 043802. DOI: `10.1103/PhysRevA.92.043802`.

[15] Pierre-Élie Larré and Iacopo Carusotto. "Prethermalization in a quenched one-dimensional quantum fluid of light. Intrinsic limits to the coherent propagation of a light beam in a nonlinear optical fiber". In: *European Physical Journal D* 70.3, 45 (Mar. 2016), p. 45. DOI: `10.1140/epjd/e2016-60590-2`. arXiv: `1510.05558` `[cond-mat.quant-gas]`.

[16] Myrann Baker-Rasooli et al. *Observation of Jones-Roberts solitons in a paraxial quantum fluid of light*. 2025. arXiv: 2501.08383 [cond-mat.quant-gas].

[17] J. R. Abo-Shaeer et al. "Observation of Vortex Lattices in Bose-Einstein Condensates". In: *Science* 292.5516 (2001), pp. 476–479. DOI: 10.1126/science.1060182. eprint: https://www.science.org/doi/pdf/10.1126/science.1060182.

[18] Myrann Baker-Rasooli et al. "Turbulent dynamics in a two-dimensional paraxial fluid of light". In: *Phys. Rev. A* 108 (6 Dec. 2023), p. 063512. DOI: 10.1103/PhysRevA.108.063512.

[19] C. J. Pethick and H. Smith. *Bose–Einstein Condensation in Dilute Gases*. 2nd ed. Cambridge University Press, 2008.

[20] Alice Sinatra, Carlos Lobo, and Yvan Castin. "The truncated Wigner method for Bose-condensed gases: limits of validity and applications". In: *Journal of Physics B: Atomic, Molecular and Optical Physics* 35.17 (Aug. 2002), pp. 3599–3631. ISSN: 0953-4075. DOI: 10.1088/0953-4075/35/17/301. URL: http://dx.doi.org/10.1088/0953-4075/35/17/301.

[21] Pierre-Élie Larré and Iacopo Carusotto. "Prethermalization in a quenched one-dimensional quantum fluid of light: Intrinsic limits to the coherent propagation of a light beam in a nonlinear optical fiber". In: *The European Physical Journal D* 70.3 (Mar. 2016). ISSN: 1434-6079. DOI: 10.1140/epjd/e2016-60590-2.

[22] Pierre-Élie Larré and Iacopo Carusotto. "Propagation of a quantum fluid of light in a cavityless nonlinear optical medium: General theory and response to quantum quenches". In: *Physical Review A* 92.4 (Oct. 2015). ISSN: 1094-1622. DOI: 10.1103/physreva.92.043802.

[23] Pierre-Élie Larré and Iacopo Carusotto. "Optomechanical signature of a frictionless flow of superfluid light". In: *Phys. Rev. A* 91 (5 May 2015), p. 053809. DOI: 10.1103/PhysRevA.91.053809.

[24] Murad Abuzarli. "Out of equilibrium dynamics in a paraxial fluid of light". 2022SORUS161. PhD thesis. 2022. URL: http://www.theses.fr/2022SORUS161/document.

[25] V. I. Yukalov. "Structure factor of bose-condensed systems". In: *Journal of Physical Studies* 11.1 (2007), pp. 55–62. DOI: https://doi.org/10.30970/jps.11.055.

[26] Theo Torres et al. "Rotational superradiant scattering in a vortex flow". In: *Nature Physics* 13.9 (Sept. 2017), pp. 833–836. DOI: 10.1038/nphys4151.

[27] Maria Braidotti et al. *Measurement of Penrose superradiance in a photon superfluid*. Sept. 2021. DOI: 10.48550/arXiv.2109.02307.

[28] Angus Prain et al. "Superradiant scattering in fluids of light". In: *Physical Review D* 100.2 (July 2019). ISSN: 2470-0029. DOI: 10.1103/physrevd.100.024037.